Functional groups of ryanodine receptors in rat ventricular cells

V. Lukyanenko, A. Ziman, A. Lukyanenko, V. Salnikov and W. J. Lederer

Medical Biotechnology Center, University of Maryland Biotechnology Institute, Baltimore, MD 21201, USA

Ryanodine receptors (RyR2s) are ion channels in the sarcoplasmic reticulum (SR) that are responsible for Ca^{2+} release in rat ventricular myocytes. Localization of RyR2s is therefore crucial for our understanding of contraction and other Ca^{2+}-dependent intracellular processes. Recent results (e.g. circular waves and Ca^{2+} sparks in perinuclear area) raised questions about the classical views of RyR2 distribution and organization within ventricular cells. A Ca^{2+} spark is a fluorescent signal reflecting the activation of a small group of RyR2s. Frequency and spatio-temporal characteristics of Ca^{2+} sparks depend on the state of cytoplasmic and intraluminal macromolecular complexes regulating cardiac RyR2 function. We employed electron microscopy, confocal imaging of spontaneous Ca^{2+} sparks and immunofluorescence to visualize the distribution of RyR2s in ventricular myocytes and to evaluate the local involvement of the macromolecular complexes in regulation of functional activity of the RyR2 group. An electron microscopy study revealed that the axial tubules of the transverse–axial tubular system probably do not have junctions with the network SR (nSR). The nSR was found to be wrapped around intermyofibrillar mitochondria and contained structures similar to feet of the junctional cleft. Treatment of ventricular myocytes with antibodies against RyR2 showed that in addition to the junctional SR, a small number of RyR2s can be localized at the middle of the sarcomere and in the zone of perinuclear mitochondria. Recordings of spontaneous Ca^{2+} sparks showed the existence of functional groups of RyR2s in these intracellular compartments. We found that within the sarcomere about 20% of Ca^{2+} sparks were not colocalized with the zone of the junctional or corbular SR (Z-line zone). The spatio-temporal characteristics of sparks found in the Z-line and A-band zones were very similar, whereas sparks from the zone of the perinuclear mitochondria were about 25% longer. Analysis of the initiation sites of Ca^{2+} sparks within the same junctional SR cluster suggested that 18–25 RyR2s are in the functional group producing a spark. Because of the similarity of the spatio-temporal characteristics of sarcomeric sparks and ultrastructural characteristics of nSR, we suggest that the functional groups of RyR2s in the middle of the sarcomere are macromolecular complexes of ∼20 RyR2s with regulatory proteins. Our data allowed us to conclude that a significant number of functional RyR2s is located in the middle of the sarcomere and in the zone of perinuclear mitochondria. These RyR2s could contribute to excitation–contraction coupling, mitochondrial and nuclear signalling, and Ca^{2+}-dependent gene regulation, but their existence raises many additional questions.

(Resubmitted 15 May 2007; accepted 15 June 2007; first published online 12 July 2007)
Corresponding author V. Lukyanenko: Medical Biotechnology Center, University of Maryland Biotechnology Institute, 725 W. Lombard St, Room S213, Baltimore, MD 21201, USA. Email: lukyanen@umbi.umd.edu

Ryanodine receptors (RyR2s) are Ca^{2+}-permeable ion channels in the membrane of the sarcoplasmic reticulum (SR). In ventricular cardiomyocytes, RyR2s are responsible for local Ca^{2+}-induced Ca^{2+} release (CICR) from the SR (Fabiato, 1985; Inui *et al.* 1987; Lai *et al.* 1988). Ca^{2+} released from the SR activates contraction and affects other Ca^{2+}-dependent intracellular processes. Thus, the spatial distribution and organization of RyR2s is important to our understanding of cardiac cell physiology.

RyR2s are largely localized to the junctional SR (jSR) that apposes the T-tubules of the transverse–axial tubular system (TATS) and spans the junctional cleft between the T-tubule and jSR (Franzini-Armstrong, 1973; Jorgensen *et al.* 1993; Carl *et al.* 1995). In rat ventricular cells, RyR2s are grouped in clusters (Franzini-Armstrong *et al.* 1999). The distance between the membranes of the jSR and T-tubule is about 12 nm (Brochet *et al.* 2005). This small space allows effective activation of the jSR RyR2s by

 DOI: 10.1113/jphysiol.2007.136549

Ca^{2+} influx through T-tubule L-type Ca^{2+} channels during excitation–contraction coupling (Bers, 2001). Besides the jSR, RyR2s were also found to be localized in the corbular SR (cSR). The cSR is located in close proximity to Z-lines but much further from the TATS membranes than the jSR. The role of the cSR in cardiac cell physiology remains uncertain (Dolber & Sommer, 1984; Jorgensen & McGuffee, 1987; Jorgensen *et al.* 1993). The network SR (nSR) in ventricular myocytes has been reported to be nearly free of RyR2s (Jorgensen *et al.* 1993).

At least three types of recent results raise questions about this classic view of RyR2 distribution and organization. (1) Subramanian *et al.* (2001) explained the phenomenon of similar velocity of propagation of Ca^{2+} waves in transverse and longitudinal directions by hypothesizing that a significant fraction of Ca^{2+}-release units should exist between Z-lines. (2) Chen-Izu *et al.* (2006) described intercalated RyR2 clusters in cardiac cells that are interspersed between Z-lines on the cell periphery. (3) Ryanodine-sensitive Ca^{2+}-release events were recently described for regions located close to the nucleus in rat ventricular cells (Yang & Steele, 2005, 2007).

While this array of observations is provocative, each of them assumes a distinct non-classical distribution of RyR2s in ventricular cells. We employed confocal imaging of spontaneous Ca^{2+} sparks and immunofluorescence to re-examine the distribution of RyR2s. A 'typical' Ca^{2+} spark is a bright and short fluorescent signal corresponding to a transient (∼30 ms) and local (∼10 fl) elevation of $[Ca^{2+}]$ that reflects the activation of a group of 10 or more RyR2s and serves as an elementary event of SR Ca^{2+} release (Cheng *et al.* 1993; Lopez-Lopez *et al.* 1995; Györke *et al.* 1997; Lukyanenko *et al.* 2000; Sobie *et al.* 2002). In adult mammalian ventricular myocytes, SR Ca^{2+} release depends on the functional state of the RyR2s (i.e. from state of cytoplasmic and intraluminal macromolecular complexes regulating cardiac ryanodine receptor function; Bers, 2004; Györke *et al.* 2004; Wehrens *et al.* 2005). These changes in the functional activity of the RyR2s could be recorded as changes in the frequency and spatio-temporal characteristics of Ca^{2+} sparks. For example, unbinding of FKBP12.6 (calstabin-2) from RyR2s lengthens the duration of Ca^{2+} sparks (Xiao *et al.* 1997; Marx *et al.* 2000; Bers, 2004), and binding of calsequestrin significantly reduces the amplitude and frequency of Ca^{2+} sparks (Viatchenko-Karpinski *et al.* 2004; Györke *et al.* 2004). Thus, under other similar conditions, the similarity in frequency and spatio-temporal characteristics of Ca^{2+} sparks suggests similarity in the ultrastructural organization of spark-producing groups of RyR2s.

Immunofluorescence is a contemporary method to demonstrate localization of proteins within permeabilized cells. We followed two immunofluorescence protocols to determine the location of RyR2s. To reduce input from out-of-focus signal and improve localization of antigens we employed deconvolution of confocal images (Sedarat *et al.* 2004; Scriven *et al.* 2005). The multidisciplinary nature of this work allowed distinct and independent methods to complement each other.

The aim of the work presented here was to determine the location of functional groups of RyR2s in adult rat ventricular cells. Multiple complementary methods were employed to examine the location and function of the SR Ca^{2+} release channels, RyR2s. Here, we demonstrate that a significant number of functional groups of RyR2s are located at sites away from the Z-line. Possible organization and roles of these non-junctional groups of RyR2s are discussed.

Methods

Cell isolation

Single ventricular myocytes were obtained from adult male Sprague–Dawley rat hearts by enzymatic dissociation as previously described (DuBell *et al.* 2000). The animals were killed by lethal injection of Nembutal (100 mg kg^{-1} I.P.). The aorta was cannulated for Langendorff perfusion, and ventricular myocytes were isolated by a standard enzymatic technique using a Hepes-buffered solution containing (mM): NaCl 130, KCl 5.4, lactic acid 1, pyruvic acid 3, Hepes 25, NaH_2PO_4 0.33, $MgCl_2$ 1.0 and glucose 20; pH was adjusted to 7.4 with NaOH.

The coronary arteries were perfused with the above solution containing 50 mg collagenase Type II (Worthington Biochemical), 1 mg protease type XIV and 50 μM $CaCl_2$. After 10 min of perfusion, the ventricles were excised, minced and then gently agitated for 4 min in a digestion buffer containing 0.1 mM $CaCl_2$ and 1.0% bovine serum albumin (BSA). The cells were filtered through a 200 μm nylon mesh and then washed and resuspended in an enzyme-free buffer containing 1% BSA. After the final wash, the cells were resuspended at room temperature (21–23°C) in a Hepes-buffered Dulbecco's modified Eagle's medium with 10% fetal calf serum.

Unless specified otherwise, all chemicals were from Sigma.

Experimental solutions for permeabilized myocytes

Isolated ventricular cells were permeabilized by exposure to 0.01% saponin for 0.5 min as previously described (Lukyanenko & Györke, 1999). Tyrode solution contained (mM): NaCl 140, KCl 5.4, $MgCl_2$ 0.5, $CaCl_2$ 1, Hepes 10, NaH_2PO_4 0.25 and glucose 5.6; pH 7.3. The permeabilization solution contained (mM): potassium aspartate 100, KCl 20, MgATP 3, $MgCl_2$ 0.81 ($[Mg^{2+}]_{free} = \sim 1$ mM), EGTA 0.5, $CaCl_2$ 0.114 mM ($[Ca^{2+}]_{free} = \sim 90$ nM), Hepes 20, glutamic acid 3 and

malic acid 3, and 1% polyvinylpyrrolidone (PVP); pH 7.2. The control experimental solution contained (mM): potassium aspartate 100, KCl 20, MgATP 3, $MgCl_2$ 0.81 ($[Mg^{2+}]_{free} = \sim 1$ mM), EGTA 0.5, $CaCl_2$ 0.114 ($[Ca^{2+}]_{free} = \sim 90$ nM), Hepes 20, glutamic acid 3, malic acid 3, phosphocreatine 10, and 5 U ml^{-1} creatine phosphokinase and 1% PVP; pH 7.2. The free $[Ca^{2+}]_{free}$ and $[Mg^{2+}]_{free}$ at the given total calcium, magnesium, ATP and EGTA concentrations were calculated using WinMAXC32 2.5 (Stanford University, CA, USA). Measurements with a spectrofluorometer D-Scan (PTI, Monmouth Junction, NJ, USA) and the Ca^{2+} indicator fura-2 (TefLabs, Austin, TX, USA) showed that real $[Ca^{2+}]_{free}$ in the experimental solution was ~100 nM.

Electron microscopy

Tissue. Pieces of rat heart were fixed in 0.5% glutaraldehyde, 2% paraformaldehyde and 0.025% $CaCl_2$ in 0.05 M sodium cacodylate buffer (pH 7.4), then exposed to a microwave oven (Laboratory Microwave Processor, Model 3440 PELCOTM, Ted Pella, Inc., Redding, CA, USA) for 15–20 s. After primary irradiation, tissue samples were kept in the same fixative solution for 5 min at 4°C, then rinsed in buffer, transferred into 0.5% OsO_4 in 0.05 M sodium cacodylate buffer (pH 7.4), and re-exposed to microwave radiation. After secondary microwave irradiation, the tissue was kept in the same fixative solution for 1 h at 4°C.

Cells. To get longitudinal sections, isolated rat ventricular cells were allowed to attach to coverslips covered with laminin in Tyrode solution for 10 min before fixation. The Tyrode solution was then replaced by 0.1 M sodium cacodylate buffer (pH 7.4) containing 6% glutaraldehyde and 2% paraformaldehyde for 1 or 20 min at room temperature. After fixation, the cells were rinsed twice with 0.2 m sucrose buffer and postfixed with 1% osmium in s-Colloidine buffer (Electron Microscopic Science, Hatfield, PA, USA) for 1 h at 4°C. Then samples were stained *en bloc* (2% uranyl acetate in 50% ethanol) for 1 h.

After dehydration in an alcohol series, the samples (both tissue and cells) were embedded in LR White resin (Ted Pella, Inc.). Polymerization took 12 h at 60°C. Ultrathin sections (~80 nm) were obtained with a LKB III microtome (LKB, Uppsala, Sweden), collected on Formvar-coated nickel grids, and stained for 15 min with 2% aqueous uranyl acetate and then for 2 min with lead citrate at room temperature. Sections were examined at 60 kV with a Zeiss electron microscope EM 10C/EM 10 CR (Zeiss, Goettingen, Germany).

Localization of Ca^{2+} sparks

Permeabilized ventricular myocytes were incubated for at least 5 min with 25 μM fluo-3 (pentapotassium salt; Biotium, Inc., Hayward, CA, USA), and 0.1 μM BODIPY TR-X ryanodine (BTR) (Molecular Probes Inc., Eugene, OR, USA). These fluorescent dyes were excited by argon (488 nm; fluo-3) or HeNe (543 nm; BTR) laser illumination. Fluorescence signals were recorded with a Laser Scanning Confocal System (LSM 510, Carl Zeiss, Germany) equipped with a C-Apochromat 63 × /1.2 W corr objective. Fluorescence was measured at wavelengths of > 505 nm (fluo-3) and > 560 nm (BTR). All measurements were done from optical slices < 1 μm with a laser beam power of ~0.08 mW. Note that BTR itself produced no fluorescence at the used concentrations (0.1 μM), when excited at 488 nm. In our preliminary experiments we used a 100 times higher concentration of BTR (10 μM); however, the signal recorded with 'spark parameters' (i.e. absorbtion/emission, 488/505 nm; optical slice, < 1 μm; maximal gain) was not different from noise of the system.

For *x–y* images, every line was scanned for 15.4 ms (mean of $n = 8$ scans) with a pixel size of 0.03 μm × 0.03 μm (at zoom = 10). Under these recording conditions, sparks could be seen on the images as 2 pixel-wide lines. To localize sparks found with fluo-3 (argon laser), the locations of their geometrical centres were marked with circles on corresponding BTR *x–y* images (HeNe laser).

Due to our approach combining the *x–y* and *x–t* modes, the Ca^{2+} spark found on the images could be both out-of-focus and out-of-line of scan (Pratusevich & Balke, 1996). Note that a major task for this study was to localize a Ca^{2+} spark along a sarcomere (i.e. on the *X* axis). Because the same place was scanned 16 times, we obtained complete information about the width of the 30 ms Ca^{2+} event. It is known that the Ca^{2+}–dye complex diffuses in ventricular cells with the same velocity longitudinally and transversely (Subramanian *et al.* 2001). Therefore, the geometrical centre of the Ca^{2+} spark should correspond to the *X* coordinate of the Ca^{2+} flux underlying the Ca^{2+} spark. Although the *Y* and *Z* coordinates could be ignored for this study, we took into account only the brightest 20% of all Ca^{2+} sparks recorded from the smallest possible optical slice (see above). This allowed us to minimize input from out-of-line and out-of-focus sparks. As a result, sparks were not recorded inside mitochondria at a depth of more than 0.1 μm. In the middle of the sarcomere this corresponds to error in the *Y* coordinate. If so, the *Z* error in localization of the Ca^{2+} sparks for 20% brightest events must be about half of error in *Y* direction (Pratusevich & Balke, 1996). Therefore, we can conclude that our approach allowed for the determination of the *X* coordinate of Ca^{2+} sparks; however, the Ca^{2+} sparks could

be ∼100 nm out of the line of scan and ∼50 nm out of the optical slice (this is smaller than the size of two RyR2s).

Spatio-temporal characteristics of Ca^{2+} sparks

Ca^{2+} spark characteristics in permeabilized ventricular cells were measured in *x*–*t* (line scan) mode as previously described (Lukyanenko *et al.* 2000). An analog recording of fluorescence intensity during each scan was digitized into 512 pixels, giving a nominal pixel dimension of 0.29 μm. Line-scan images (*x*–*t* mode) were acquired at a rate of 520 Hz (1.92 ms per line scan) and stored in tif-format. All line-scan images of sparks were obtained from the smallest possible optical slices ($< 1\ \mu$m at laser beam power of ∼0.08 mW) by scanning the cells longitudinally.

Immunofluorescence

Freshly isolated ventricular myocytes were fixed in 2% paraformaldehyde for 15 min. Following fixation, cells were washed 4 times for 15 min with PBS. Cells were blocked and permeabilized in a solution of 1% BSA, 1% NGS and 5 mg ml^{-1} saponin in PBS for 1 h. Following blocking, primary antibodies (diluted 1 : 100) in 1% BSA and 1% NGS in PBS were added to cells overnight at 4°C. After primary antibody incubation, cells were washed 4 times for 30 min with 1% BSA and 1% NGS in PBS. Goat anti-mouse or goat anti-rabbit secondary antibodies conjugated to Alexa 488 (diluted 1 : 500) were applied to the cells for 2 h at room temperature. Following secondary antibody exposure, cells were washed 3 times for 30 min with 1% BSA and 1% NGS in PBS, then twice for 15 min in PBS. Immunostained myocytes were then mounted on glass slides using Slow Fade Light. Negative controls were produced by using the same protocol without the use of a primary antibody.

Primary antibodies. We used monoclonal Anti-RyR2 MA3-916 (Affinity BioReagents Inc., Golden, CO, USA); polyclonal anti-calsequestrin (Swant, Bellinzona, Switzerland); monoclonal anti-α tubulin 12G10 (Developmental Studies Hybridoma Bank, Iowa City, IA, USA) and polyclonal anti-junctophilin2 (Invitrogen, Carlsbad, CA, USA).

Image collection and processing. Immunofluorescent images were collected using a Carl Zeiss Laser Scanning Confocal System (LSM 510, equipped with a C-Apochromat 63 × /1.2 W corr objective) with excitation at 488 nm and a long-pass filter of 505 nm. Deconvolution of immunofluorescence images was performed to clarify the distribution of the antibodies. High resolution *z*-stacks (stacks with a maximum pixel size of 0.1 μm × 0.1 μm × 0.2 μm) were processed using Volocity 3.5.1 (Improvision, Cambridge, MA, USA). Images were first passed through a fine (3 pixel × 3 pixel) Gaussian filter to remove scattered light. Then, images were deconvolved using the iterative restoration algorithm developed by Improvision Inc. (Lexington, MA, USA) (based on published maximum entropy techniques) to increase resolution in *X*, *Y* and *Z*. Representative images (see Figs 4 and 5) show the typical fluorescent pattern for 50–100 cells.

Experiments were performed at room temperature. Data were expressed as means ± S.E.M. Comparisons were performed using Student's *t* test, and differences were considered significant when $P < 0.05$.

Results

The aim of the work presented here was to determine the location of functional groups of RyR2s in adult rat heart cells. Multiple complementary methods were employed to examine the location and function of the SR Ca^{2+} release channels, RyR2s.

Revealing the ultrastructure features of the SR with electron microscopy

In ventricular cells, the SR is located between mitochondria and myofibrils or T-tubules (Sommer & Johnson, 1968; Fawcett & McNutt, 1969; Dolber & Sommer, 1984; Frank, 1990). Recently, we confirmed the existence of connecting pillars between the jSR and mitochondrial outer membrane by adding 3 nm particles before preparation of ventricular cells for electron microscopy (i.e. *in vivo*; Parfenov *et al.* 2006; Salnikov *et al.* 2007). This allowed us to suggest that the SR could be attached to mitochondria as to most stable structures within the contracting cells at least near the Z-line. To clarify distribution of the SR around mitochondria, we employed embedding in LR White resin.

Although conventional electron microscopy fixation followed by Epon embedding is best for preserving and imaging intracellular structures (Fawcett & McNutt, 1969; Maunsbach & Afzelius, 1999; Brochet *et al.* 2005), in comparison to water-soluble resins it significantly restricts penetration of contrasting agents into the body of the slice (Shalla *et al.* 1964; Peters *et al.* 1971). Therefore, to better visualize the SR, we used conventional fixation followed by embedding in water-soluble LR White resin (Newman & Hobot, 1993; Parfenov *et al.* 2006; Salnikov *et al.* 2007).

Despite the expected reduction in structure quality produced by LR White (Maunsbach & Afzelius, 1999), this kind of embedding allowed the visualization of ventricular cell ultrastructure. Figure 1*A* shows inter-myofibrillar mitochondria (IMFMs), nSR and jSR, TATS, Z-lines, M-lines, and I- and A-bands of the sarcomere. The contrasting of the entire thickness of the slice allowed us

to see overlapping nSR and mitochondrial cristae or nSR and myofibrils (Fig. 1*B*).

The most important finding here is the platforms created by junctions of nSR branches (Fig. 1*C*). If RyR2s in the cluster are organized in a checkerboard order (Yin *et al.* 2005; Parfenov *et al.* 2006), such platforms could carry group of ∼20 RyR2s. We found such platforms mainly in the middle of the sarcomere (M line). Because of multiple junctions, the nSR at the level of the M line was named M-rete (Dolber & Sommer, 1984). It is interesting that in our LR White electron microscopy images, M-rete often filled mitochondrial invaginations as shown for two mitochondria in Fig. 1*D*. This demonstrates that the nSR has tight connections with the mitochondrial outer membrane. This connection could have a biological relevance because mitochondria are relatively stable structures in the contracting cells. However, if the SR has connections to mitochondria both near the Z-line (jSR) and the M line (nSR) it has to wrap around them. Figure 1*E* shows an oblique section through three mitochondria. The nSR is seen as rays around them. This supports the hypothesis that the nSR wraps around mitochondria rather than the myofilament bundle, as can be seen in classical schematic representations (Fawcett & McNutt, 1969). Thus, mitochondria could be the best reference structure to localize functional groups of RyR2s independently of their location in the SR network.

If RyR2s are located in the middle of a sarcomere, they could be visualized after conventional fixation followed by Epon embedding (Brochet *et al.* 2005; Parfenov *et al.* 2006). This embedding allows the ultrastructure to be seen much better than following embedding in the LR White resin (Maunsbach & Afzelius, 1999; Parfenov *et al.* 2006). We expected to find structures similar to feet (structures which were identified as RyR2s by Franzini-Armstrong (1973) to be free of contacts, as shown for corbular SR (Dolber & Sommer, 1984), or between SR and longitudinal tubules of TATS (i.e. the jSR in the middle of the sarcomere). In other words, we were looking for structures similar to cSR or jSR in the middle of a sarcomere. Figure 2*A* shows part of the nSR containing structures that could be considered as RyR2s (inset; arrowheads) due to the clear checkerboard pattern. They are located within the edges of the nSR and are similar in size to feet in the junctional cleft (Fig. 2B; arrowheads). Although similar structures could sometimes be seen outside the nSR, there are two reasons why we provide the image showing them inside the nSR. First, they keep the checkerboard order, while curvature of SR tubes has to mask the pattern and such structures outside nSR could be mistaken for similarly sized glycogen granules or ribosomes (Fawcett & McNutt, 1969). Second, even embedding in Epon sometimes shows an overlay of structures within the slice due to the penetration of contrasting agents (Shalla *et al.* 1964; Peters *et al.* 1971). Thus, the particles could be located outside the SR tubule and be

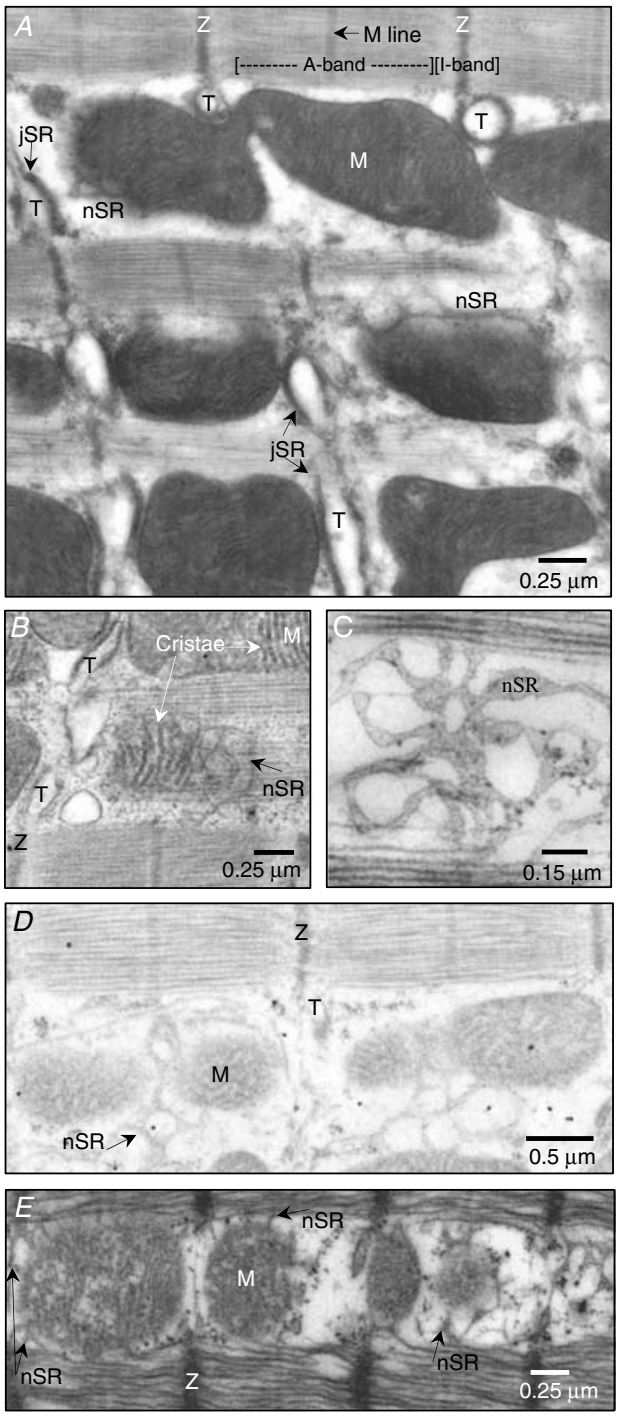

Figure 1. Sarcoplasmic reticulum in rat ventricular cells
The electron micrographs (longitudinal ultrathin section) show ventricular cell ultrastructure using conventional fixation and polymerization in acrylic LR White Resin. *A*, oblique section in tissue samples shows localization of junctional SR (jSR) and network SR (nSR) in relation to T-tubules and mitochondria (M). *B–D*, nSR. Isolated cells. B, in the centre of the micrograph nSR is seen together with mitochondrial cristae or with contractile elements. C, junctions of branches of the nSR create platforms that could carry small group of RyR2s. D, an nSR fills mitochondrial invaginations. E, oblique section through three mitochondria shows nSR wrapping around them. jSR, junctional SR; nSR, network SR; M, mitochondrion; T, T-tubule of TATS; Z, Z-line.

seen together with the SR. However, in this case they can be located between nSR and axial tubule of TATS.

To better visualize connections between the SR and TATS membranes, we studied TATS contacts on images after Epon embedding. We studied 738 electron micrographs of ventricular cells ($\times$ 60 000–100 000) where the jSR around T-tubules was clearly seen; however, we found only eight micrographs clearly showing axial TATS tubules entering T-tubules and they did not have contacts with the SR. It is interesting that we did not find axial tubules of TATS within the same ultrathin section between two T-tubules, unless the section was about 30 deg oblique. This was confirmed by contrasting of TATS membranes with tannic acid (10 cells; data not shown). These images demonstrated multiple cuts through the axial TATS tubules around IMFMs at the level of the A-band.

A representative electron micrograph (Fig. 3) shows the ultrastructure of an axial TATS tubule from an intact ventricular cell. The jSR on the micrograph could be seen only at the level of the Z-line (thick black arrows) while

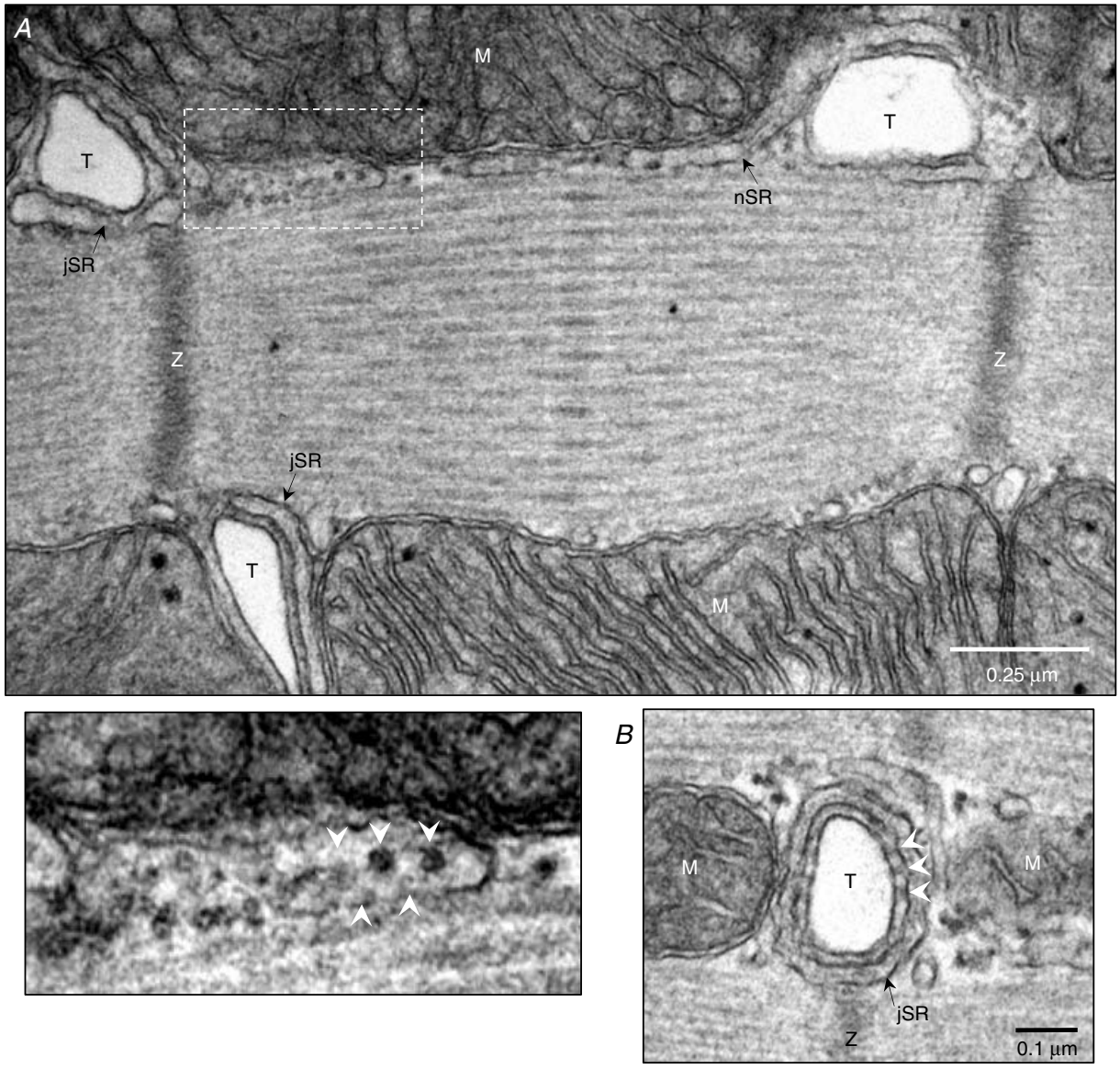

Figure 2. Distribution of possible RyR2s in rat ventricular cells
The electron micrographs (longitudinal ultrathin section) show ventricular cell ultrastructure using conventional fixation and polymerization in Epon. Slightly oblique longitudinal ultrathin section, 2.5% glutaraldehyde for 3 h. Isolated intact cell. *A* and *B*, these electron micrographs show possible RyR2s that can be attributed to network (*A*) or junctional (*B*) SR. Inset at higher magnification shows the area marked with the dashed line. T, T-tubules; nSR, network sarcoplasmic reticulum; jSR, junctional SR; M, mitochondrion; Z, Z-line; arrowheads, possible RyR2s.

near the middle part of the A-band it has a connection to the outer mitochondrial membrane rather than to the SR (see inset; black arrows).

Our images showed only two structures similar to jSR in the middle of the sarcomere and no jSR between perinuclear mitochondria. Therefore, we conclude that jSR is absent from both the perinuclear zone and the A-band of the sarcomere.

Localization of RyR2s with immunofluorescence

To localize RyR2s within ventricular cells, we employed two kinds of immunofluorescence imaging methods using primary antibodies ABR MA3-916 and secondary antibodies conjugated to Alexa 488. Figure 4 shows representative images from cells permeabilized *in vivo* ($n = 3$ experiments; 30 cells) in the presence (Fig. 4*A*) and absence (Fig. 4*B*) of the primary antibody. The permeabilization was confirmed with fluo-3 as previously described (Lukyanenko & Györke, 1999). Because the cells were 'alive' during these experiments, we restricted the time of exposure and washout for each antibody to 30 min. To facilitate penetration of antibody into the cell, we increased the time for permeabilization by a factor of two. As can be seen in Fig. 4*A* and *B*, the fluorescence from cells with primary antibodies was much higher. Figure 4*A* shows transverse bright stripes (identified by the letter 'Z' marking the Z-line) and less-bright marks between them (arrows). Arrows point to the immunofluorescence of RyR2s in the centre region of A-band (Fig. 4*A*). This suggests that RyR2s can be colocalized with nSR.

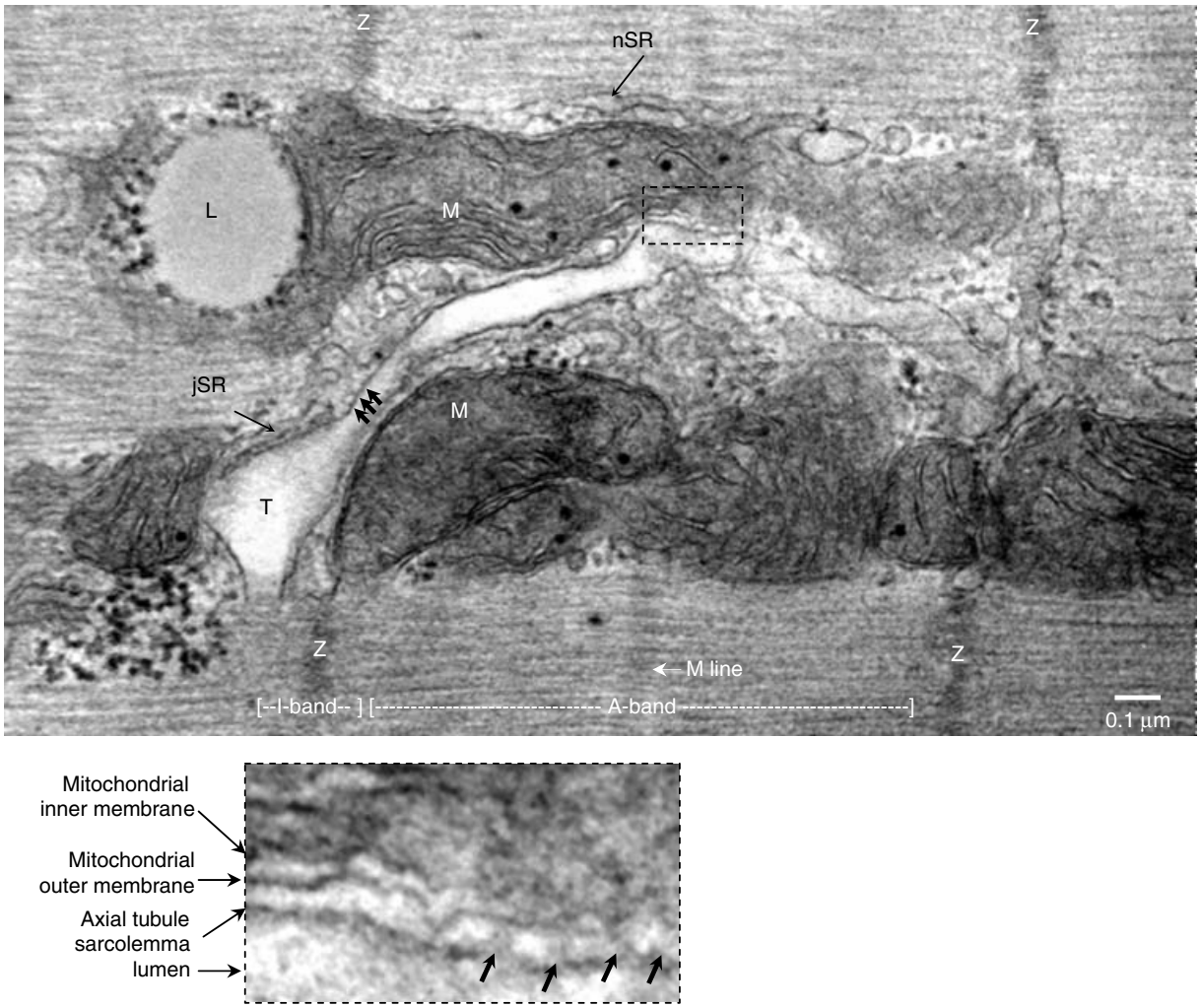

Figure 3. Axial tubule of the transverse–axial tubular system (TATS)
Slightly oblique longitudinal ultrathin section, 2.5% glutaraldehyde for 3 h, Epon embedding. Isolated intact cell. This electron micrograph shows an axial tubule of TATS. Arrows show bridges between the tubule membrane and jSR (thick arrows) and outer mitochondrial membrane (marked area). Inset at higher magnification shows the area marked with dashed line. Arrows show possible contacts between axial tubule of TATS and mitochondrion. T, T-tubules; nSR, network sarcoplasmic reticulum; jSR, junctional SR; M, mitochondrion; Z, Z-line; L, lipid droplet.

To allow the antibodies to penetrate deeper into the cell, we performed experiments with cells fixed in paraformaldehyde (Fig. 4*C* and *D*). The cells were permeabilized with saponin and left overnight with primary antibodies against RyR2 (MA3-916; $n = 3$ experiments; 30 cells each). The images were obtained following deconvolution, a method that involves the gathering of high resolution z-stacks (0.2 μm step) and using that image stack along with the point spread function (PSF) of the lens to computationally remove out-of-focus light (see Methods). The resulting images demonstrated the distribution of antibodies primarily along Z-lines;

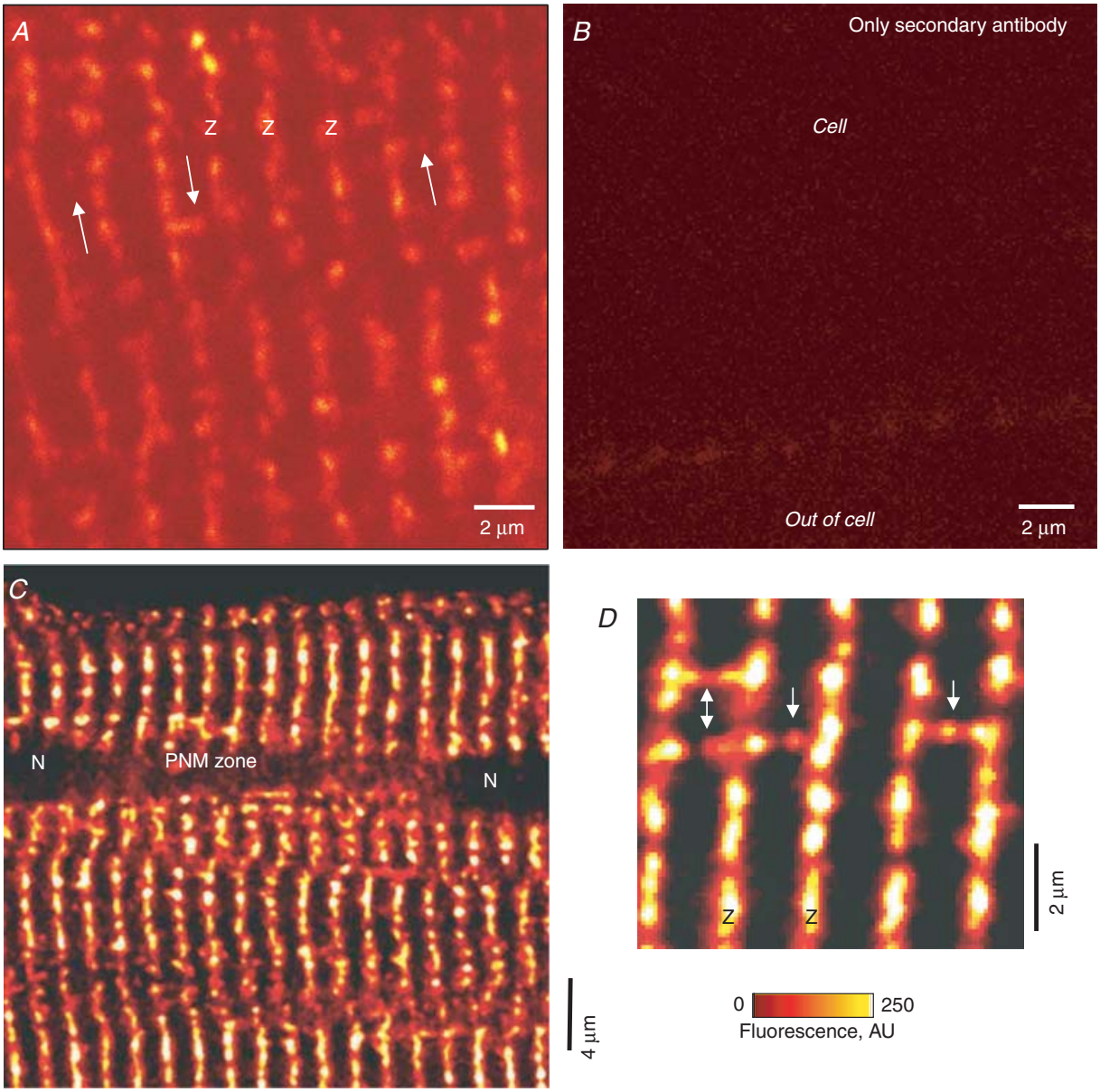

Figure 4. Distribution of RyR2s marked with MA3-916 (ABR) in permeabilized ventricular cells
A–D, immunofluorescence labelling. *A* and *B*, live cells were permeabilized with saponin *in vitro*. Then the cells were incubated for 30 min with (*A*) and without (*B*) primary antibody. After a 30 min washout, the cells were incubated for 30 min with secondary antibody conjugated to a fluorescent probe and again washed-out for 30 min. *C* and *D*, representative images of cells permeabilized with saponin after fixation in paraformaldehyde. The cells were incubated overnight with primary antibody. *D*, different region of the cell presented in *C* and with higher resolution. Images are deconvolved from 3-D stack. Thickness of the optical slices for *C* and *D* was ~0.7 μm. Z-lines were marked on the images according to corresponding images in transmitted light. Z, Z-line; arrows show labelling in M band (between Z-lines); PNM, perinuclear mitochondria; N, nucleus.

however, some longitudinal lines of fluorescence were also clearly seen (Fig. 4*D*; arrows).

To exclude any impact from non-specific labelling, we performed similar immunolabelling for a protein associated structurally and functionally with RyR2s, calsequestrin (Jones *et al.* 1995; Sitsapesan & Williams, 1997; Györke *et al.* 2004). Figure 5*A* shows both transverse and longitudinal labelling for calsequestrin after deconvolution ($n = 6$). Control experiments were carried out using only secondary antibody (Fig. 5*B*; $n = 6$) and these revealed no signal. Other proteins unrelated to RyR2 (such as the cytoskeletal protein α-tubulin) were distributed as expected and differently from calsequestrin or RyR2s (Fig. 5*C*; $n = 6$). These control experiments supported our hypothesis that RyR2s can be colocalized with nSR.

Comparison of spontaneous Ca^{2+} sparks produced in different cellular subdomains

The A-band RyR2s (identified above by immunofluorescence) may be organized into groups that can support an elementary Ca^{2+} release (i.e. a Ca^{2+} spark) (Cheng *et al.* 1993; Bhat *et al.* 1999; Bridge *et al.* 1999; Lukyanenko *et al.* 2000; Sobie *et al.* 2002). Previously, we showed that groups of RyR2s that produce Ca^{2+} sparks probably contain about 10–20 functional RyR2s (Lukyanenko *et al.* 2000). These groups are much smaller than rat jSR clusters (100–300 RyR2s; Franzini-Armstrong *et al.* 1999; Chen-Izu *et al.* 2006; Soeller *et al.* 2006) and could be located on SR platforms in the middle of a sarcomere (see above; Fig. 1*C*).

To localize Ca^{2+} sparks, the ventricular cells were loaded with a Ca^{2+}-sensing fluorescent probe (as fluo-3) and a marker for referral ultrastructure. We tested markers to two different structures, T-tubules, the periphery of which (Z-line zone) was shown to have abundant RyR2s, and mitochondria, which are wrapped by the SR (see above). We performed preliminary experiments marking both T-tubules and RyR2s. To mark the T-tubules, we used di-8-ANEPPS (absorbance/emission, 498/730 nm; $n = 3$; data not shown). However, the complicated 3-D structure of TATS (Soeller & Cannell, 1999) resulted in multiple false referral points, making data interpretation very difficult.

To mark RyR2s directly, we used two different fluorescent probes: (1) antibodies to RyR2s conjugated to Alexa Fluor 633 (secondary goat anti-mouse antibody; absorbance/emission, 630/665 nm; $n = 4$; data not shown); and (2) BTR (absorbance/emission, 545 nm/650 nm). Exposure for 1 h to the antibody significantly reduced the quality of Ca^{2+} sparks and provided us with insufficient data to make any conclusions. The BTR was developed to mark RyR2s directly and we

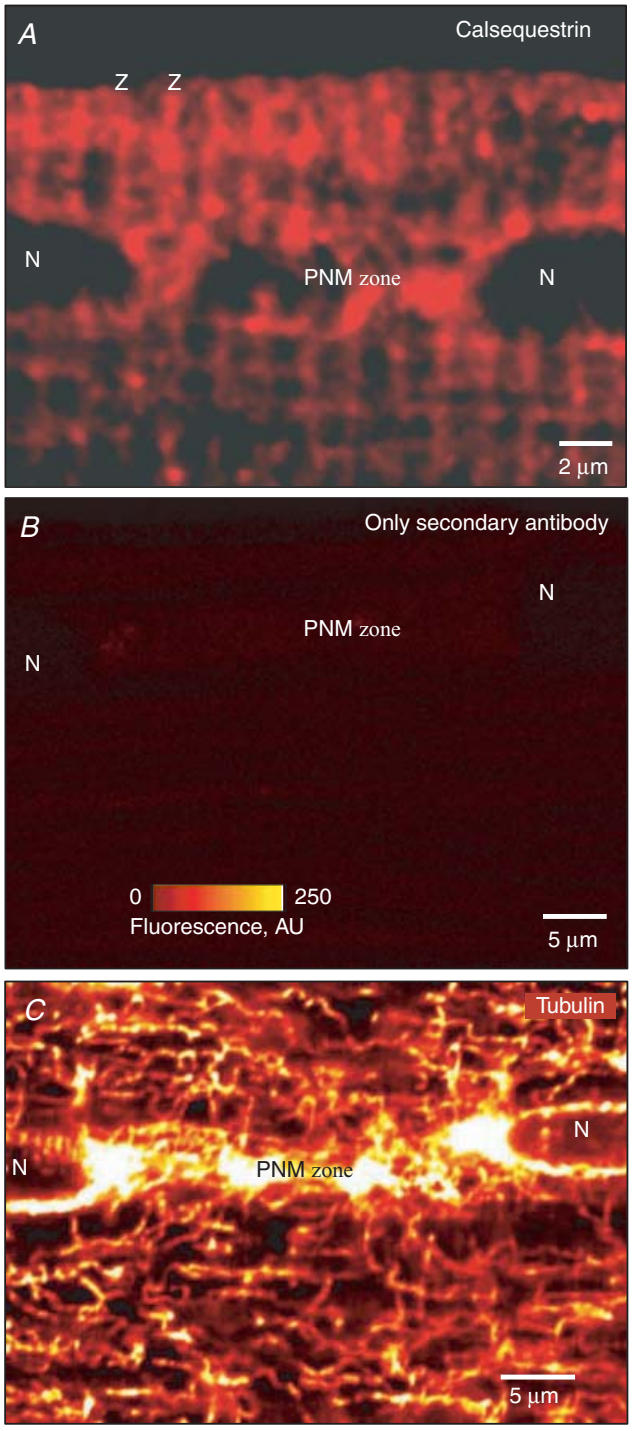

Figure 5. Distribution of calsequestrin and α-tubulin in ventricular cells
Immunofluorescence labelling. Representative images of cells permeabilized with saponin after fixation in paraformaldehyde. The cells were incubated overnight with primary polyclonal antibody against calsequestrin (*A*) or anti-α-tubulin (clone 12G10, (*C*). The primary antibody was diluted 1 : 100 and the secondary (goat anti-rabbit conjugated to Alexa 488) was diluted 1 : 500 (*A*–*C*). *A*, image is deconvolved from a 3-D stack. *B*, only secondary antibody was added to cells. Secondary antibody was diluted 1 : 200. Z, Z-line; PNM, zone of perinuclear mitochondria; N, nucleus.

expected (1) to see the BTR fluorescence along Z-lines (concentrated around T-tubules), and (2) that centres of mass of Ca^{2+} sparks will always be colocalized with areas marked by BTR. Surprisingly, our preliminary experiments showed that BTR labels mitochondria rather than RyR2s. Figure 6*A* shows that BTR (red) and antibodies to RyR2 (blue) marked different intracellular structures. The antibody marked the Z-lines, whereas BTR marked mitochondria. Only increasing BTR concetration to 10 μM allowed visualization of the Z-lines (data not shown). The addition of fluo-3 under these conditions (Fig. 6*B*) did not reveal spontaneous Ca^{2+} sparks at this concentration of BTR ($n = 5$ experiments). The inhibitory effect of 10 μM BTR on Ca^{2+} sparks suggests that molecules of BTR had also found their targets, RyR2s.

Within 10 min, the BTR filled the mitochondria entirely (Fig. 6*C*) and revealed Z-lines only in negative relief (Fig. 6*D* and *E*). This distribution of BTR could mean that BTR enters the mitochondrial intermembrane space. Based on our experiments with isolated cardiac mitochondria and membrane-impermeant fluorescent probes, we suggest that the small molecular size of BTR allowed it to pass through the mitochondrial voltage-dependent anion channel (VDAC) as we showed earlier for the salt form of fluo-3 (Chinopoulos *et al.* 2005).

To check this hypothesis, we performed similar experiments (Fig. 7) with a larger BTR analogue, BODIPY TR-X ivermectin (molecular weight, 1400). Ivermectin selectively binds to sarcolemmal glutamate-gated Cl^- channels in invertebrate muscle cells and with low affinity

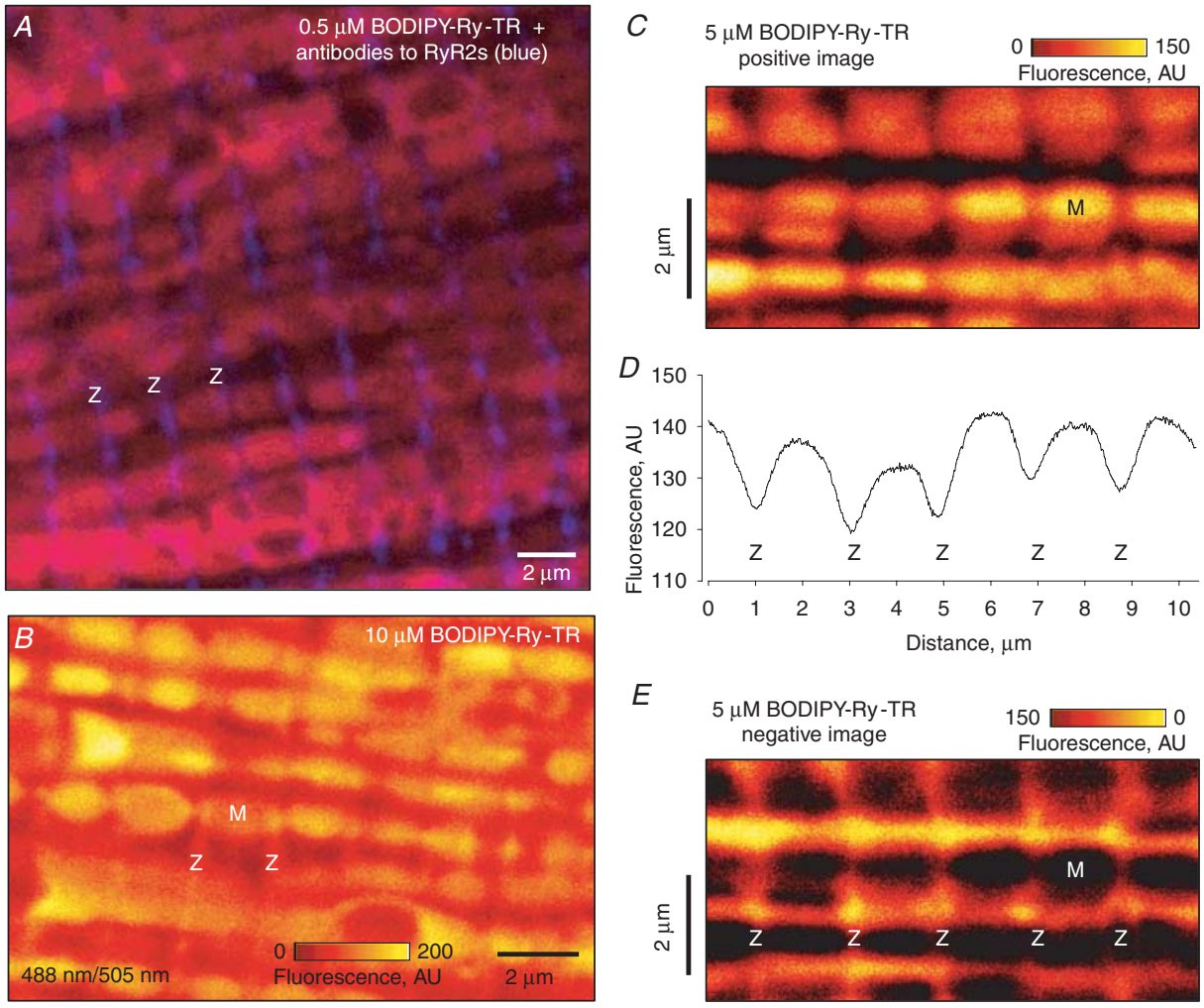

Figure 6. Spatial distribution of BODIPY TR-X ryanodine (BTR) in permeabilized ventricular cells
A, co-labelling with RyR2 antibody conjugated to Alexa Fluor 488 (blue) and 0.5 μM BTR (red). Excitation, 488 and 543 nm; emission, > 505 and > 560 nm, respectively. *B*, ventricular cell was pretreated for 10 min with 10 μM BTR and 5 min with 25 μM fluo-3 (pentapotassium salt). *C–E*, unique properties of BTR could be used to visualize Z-lines in negative relief. *C*, the cell was pretreated for 10 min with 5 μM BTR. *D*, the graph shows the average fluorescence (profile) for C. *D*, inverted image of distribution of BTR presented in *C*. Excitation/emission, 488/505 nm; optical slice < 1 μm. Z, Z-line; M, mitochondrion.

to neuronal acetylcholine, glutamate and GABA receptors, and to SERCA in rabbit skeletal muscle fibres (IC_{50}, 7 μM; Bilmen *et al.* 2002). Although we preincubated permeabilized cells with 1 μM BODIPY TR-X ivermectin (Fig. 7*A*), it induced only minor fluorescence (at least five times less than 0.1 μM BTR; Fig. 7*B* and *C*). This supported our suggestion regarding a VDAC-dependent mechanism of BTR penetration into the mitochondria.

We concluded that BTR cannot be used as a marker of RyR2s in cardiac cells. However, BTR marked mitochondria much better than the mitotracker CellTrace BODIPY TR methyl ester (Molecular Probes Inc.; data not shown). Therefore, we used its unique fluorescent properties only to mark mitochondria and to outline the Z-lines as shown above. To localize Ca^{2+} sparks, we pretreated permeabilized ventricular cells with 0.1 μM BTR (to prevent the inhibitory effect of BTR on RyR2s) and 25 μM fluo-3. The sparks could be seen on x–y confocal images as horizontal bright lines (Fig. 8*A*). It was shown

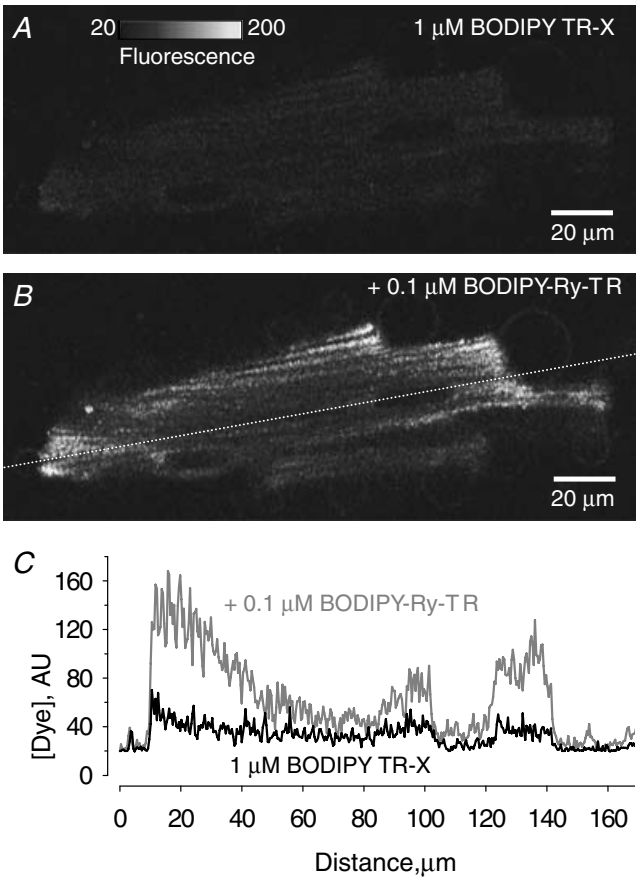

Figure 7. Spatial distribution of BODIPY TR-X ivermectin in permeabilized ventricular cells
A and *B*, ventricular cell pretreated for 15 min with 1 μM BODIPY TR-X ivermectin before (*A*) and 15 min after (*B*) addition of 0.1 μM BTR to the bathing solution. Excitation/emission, 543/650 nm. *C*, the graph shows fluorescence profiles for *A* (black) and *B* (grey) taken as shown with dotted line in *B*.

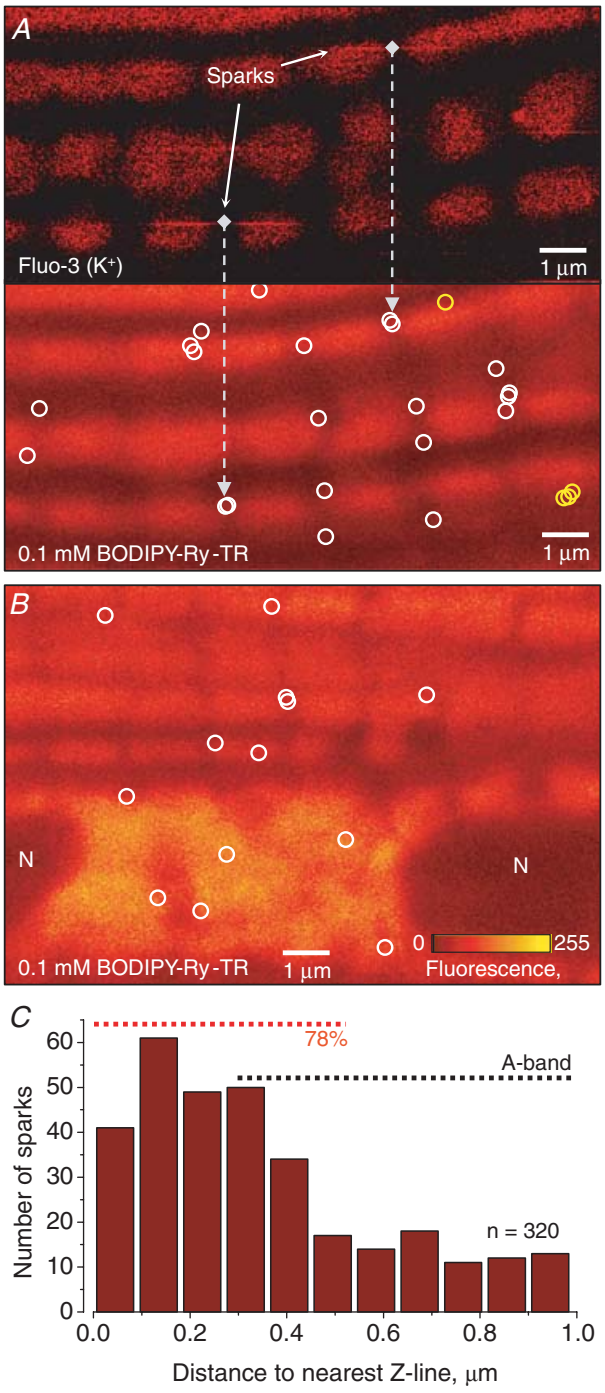

Figure 8. Spatial distribution of spontaneous Ca^{2+} sparks in permeabilized ventricular cells
A, to localize Ca^{2+} sparks, the permeabilized cells were pretreated with 0.1 μM BTR and fluo-3 (pentapotassium salt). The same area of a ventricular cell was visualized with excitation/emission, 488/505 nm (upper panel) or 543/650 nm (lower panel). Centres of spark lines found with fluo-3 were marked with circles on corresponding images in BTR as shown on lower panel. Yellow circles represent sparks from the A-band. *B*, representative image of cell showing distribution of spontaneous sparks in the zone of perinuclear mitochondria. Optical slice, < 1 μm. Note, the thickness of the slide permits mitochondria to be seen together with the surrounding SR. N, nucleus. *C*, the graph shows histogram of spark distribution as spark number against the distance from nearest Z-line.

that the Ca^{2+}–dye complex diffused isotropically (Subramanian *et al.* 2001). Therefore, we used the geometric centre of the spark to find the coordinates of its 'site of origin' on the corresponding image with BTR.

We located the positions of 430 spontaneous Ca^{2+} sparks. The sparks were localized mainly in close proximity to mitochondria in the intermyofibrillar and perinuclear zones (Fig. 8*B*) and zones of subsarcolemmal mitochondria (SSM; data not shown). Area densities of grouped RyR2s producing Ca^{2+} sparks (so called 'hot spots') in the zones were very similar (0.08 ± 0.02 and 0.08 ± 0.03 spots μm^{-2} for zones of perinuclear and subsarcolemmal mitochondria 0.06 ± 0.02 spots μm^{-2} for IMFM zone; $n = 3$–16).

About 80% (of 320) spontaneous sparks from the zone of IMFMs were located primarily within the 500 nm band along the Z-lines. The graph presented on Fig. 8*C* shows the distribution of the sparks along half of the sarcomere length. Note that about 20% of sparks are almost homogeneously distributed in the middle of A-band (black dotted line represents half of the band). Similar data were recorded in three other experiments when we used Cell Trace BODIPY or antibodies to RyR2 (data not shown) as intracellular markers of mitochondria or Z-lines.

Characteristics of spontaneous Ca^{2+} sparks from different cell subdomains

Spark spatio-temporal characteristics depend on multiple regulatory proteins attached to RyR2s from both the sarcoplasmic and intraluminal sides (Marx *et al.* 2000; Bers, 2004; Györke *et al.* 2004; Wehrens *et al.* 2005). To find out whether groups of RyR2s are organized differently in different regions of the cell, we derived spatio-temporal characteristics of Ca^{2+} sparks from events recorded in *x*–*t* mode. For this, ventricular cells were pretreated for at least 5 min with 0.1 μM BTR and visualized in *x*–*y* mode (Fig. 9*A*; left panel). Then one line was picked up (Fig. 9*A*; left panel; marked with dots) for scanning (Fig. 9*A*; right panel). After recording of sparks, an additional 10 000 repetitive line scans were made to mark a scanned line and locate it on the *x*–*y* confocal image. During data analysis, recorded spontaneous Ca^{2+} sparks were localized on the line as shown and sorted by distance from the Z-line. We compared the spatio-temporal characteristics of sparks in the zone of Z-line (500 nm from Z-line), A-band zone (1 μm in the middle of the sarcomere), and the zone of PNMs (Fig. 9*B*). To reduce the input from out-of-focus sparks, we used optical slices < 1 μm for spark recording. Before each experiment, every PNM zone was checked for thickness with 0.5 μm z-stack optical slices and the experiment was done only if the thickness of the zone was 2 μm.

Representative images in Fig. 9*C* show typical sparks from the PNM and IMFM zones (scans through lines marked in Fig. 9*B*). The sparking activity on the PNM zone was about 10 times less. However, based on our morphological data this can be attributed to a much lower density of RyR2s rather than to the macromolecular organization of the groups of RyR2s producing Ca^{2+} sparks. As shown in Fig. 9*D*, the spatio-temporal characteristics of Ca^{2+} sparks (except duration) were not significantly different from those from Z-line or A-band zones, whereas sparks from the zone of perinuclear mitochondria were about 25% longer. The similarity of the spatio-temporal characteristics of sparks from Z-line or A-band zones of ventricular cells suggests a similarity in the ultrastructural organization of macromolecular regulatory complexes of the groups of RyR2s producing sparks.

Organization of groups of RyR2s producing sparks

How RyR2s within a cluster are regulated is poorly understood. In principle, the individual RyR2 that is first activated in a cluster of up to 300 or more could influence the 'centre of mass' of the resulting Ca^{2+} spark. Paradoxically, it appears to activate only 10–20 RyR2s underlying the Ca^{2+} spark (see Bers, 2001). To test whether this group is organized spontaneously around the first opened RyR2 or whether it is a structurally discrete group, we recorded 'repetitive' spontaneous sparks. If a single RyR2 spontaneously activates a group of RyR2s within the junctional cluster, we should see an equal distribution of shortest distances between spontaneous sparks. If a single RyR2 activates a discrete group of RyR2s, the mean smallest distance will give us some understanding of the group size.

Only a few sparks arose exactly in the same location, while other sparks that looked 'repetitive' were located as far as 0.2 μm from nearest spark (Fig. 10*A*). Figure 10*A* shows one or two exceptionally active clusters of RyR2s (marked with an oval). Note, although the same cluster produces multiple sparks, the place of spark origination varies. This shows that the Ca^{2+} spark could be produced by different groups of RyR2s within the same cluster.

Figure 10*B* shows the distribution of the shortest distances between sparks. The jSR can fully wrap around a T-tubule (Parfenov *et al.* 2006). If Ca^{2+} sparks belong to the same cluster, the distance between them on the *x*–*y* image cannot readily exceed 400 nm (maximal diameter of T-tubule plus two junctional cleft distances). Therefore, we measured all shortest distances between sparks that did not exceed 400 nm. On average, the shortest distance between sparks was 162 ± 9 nm ($n = 53$). This is equal to the dimensions of only three RyR2s (~27 nm each) from a section of checkered array (Yin *et al.* 2005).

Note that in the case of expected squared groups of RyR2s, the 3-D differences in spark locations could be ignored for measurements of the group size. Previously

we showed that isolated ventricular cells are flat and ultrathin sections through myocytes plated on coverslips usually are perpendicular to T-tubules (Parfenov *et al.* 2006). Therefore, optical slices in our experiments were also mainly perpendicular to T-tubules (i.e. to jSR and junctional RyR2 clusters). The diagram presented in Fig. 10*C* shows two possible views on the cluster in the Z-direction (blue and black arrows). It can be seen that, if RyR2s are combined in squared groups, the depth of origination of the spark can be ignored and the size of the side of the group will be equal ('blue' direction) or smaller ('black' direction) than the distance between centres of spark masses. In this case the number of sparks in the functional group could be ~18. In the case of a round group (red circles), the mean distance independent of the point of view will be equal to or smaller than the diameter of the group. For the case presented in Fig. 10*C*, the diameter of the group will be up to 212 nm (i.e. square

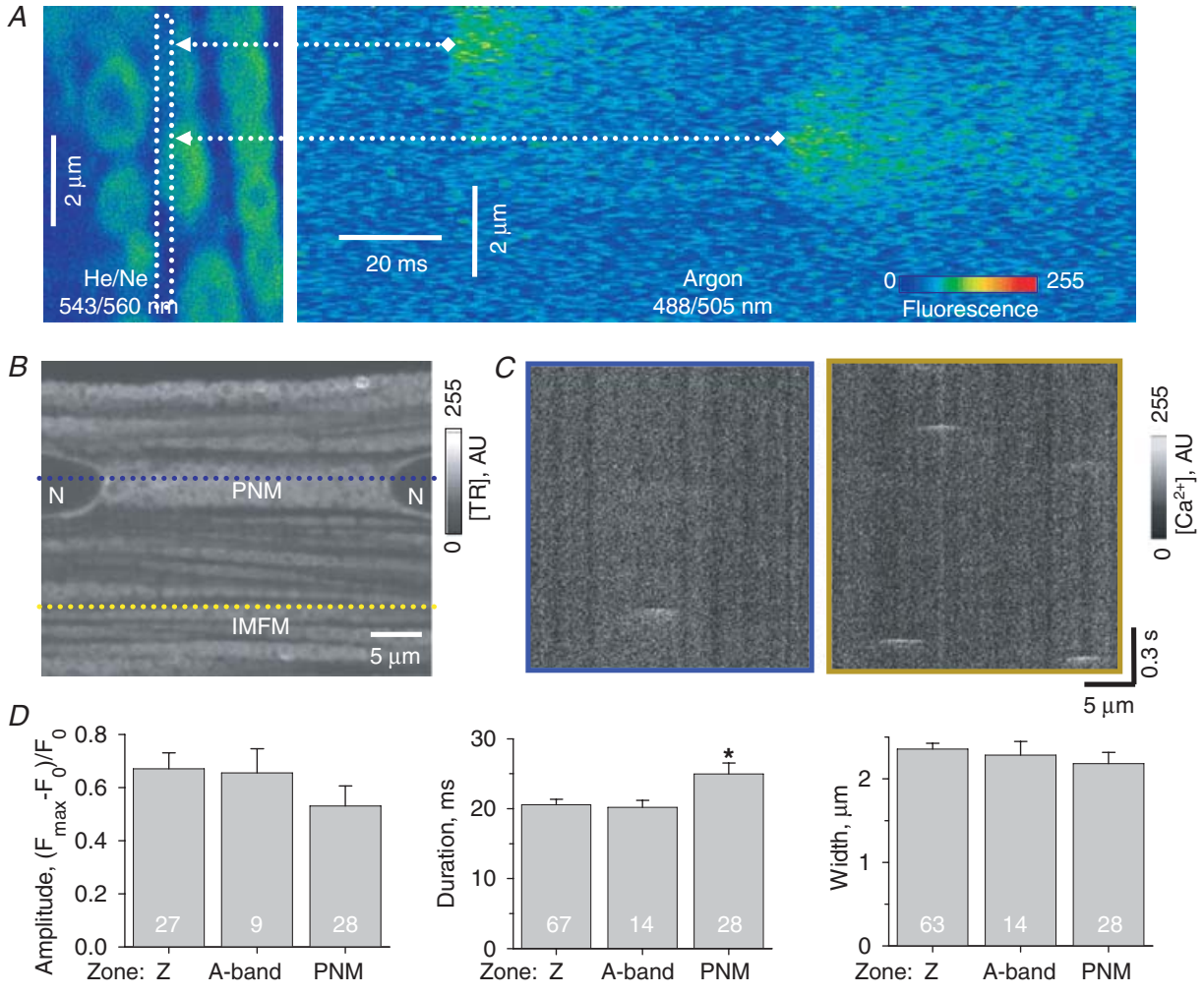

Figure 9. Spontaneous Ca^{2+} sparks in different zones of permeabilized ventricular cells
A, an example of localization of Ca^{2+} sparks. Ventricular cells were pretreated for 5 min with 0.1 μM Bodipy-TR-X ryanodine and visualized as an optical slice < 1 μm with excitation/emission, 543/560 nm in *x*–*y* mode (left panel). Then one line was picked up on the image and scanned in *x*–*t* mode with 1 ms interval with excitation/emission, 488/505 nm (right panel). Additionally, 10 000 repetitive line scans were made to mark a scanned line and locate it on the *x*–*y* confocal image (dotted square on the left panel). During data analysis, recorded spontaneous Ca^{2+} sparks were localized on the line as shown and sorted according to distance from Z-line when its location was clearly seen. *B*, representative image of ventricular cell pretreated with 0.1 μM Bodipy-TR-X ryanodine and 25 μM fluo-3 (pentapotassium salt). Excitation/emission, 543/650 nm. *C*, Ca^{2+} sparks were collected in line-scan mode scanning lines as shown in *B* in perinuclear mitochondria (PNM) zone (blue line) and IMFM zone (yellow line). Representative spark images in *C* are shown with corresponding colour of frame. *D*, spatio-temporal characteristics of sparks located in T-tubule, A-band zone or in the zone of PNM. Duration and width of sparks were measured at half of amplitude. $n = 9$–67 as marked on bars. N, nucleus; PNM, perinuclear mitochondria; IMFM, intermyofibrillar mitochondrion.

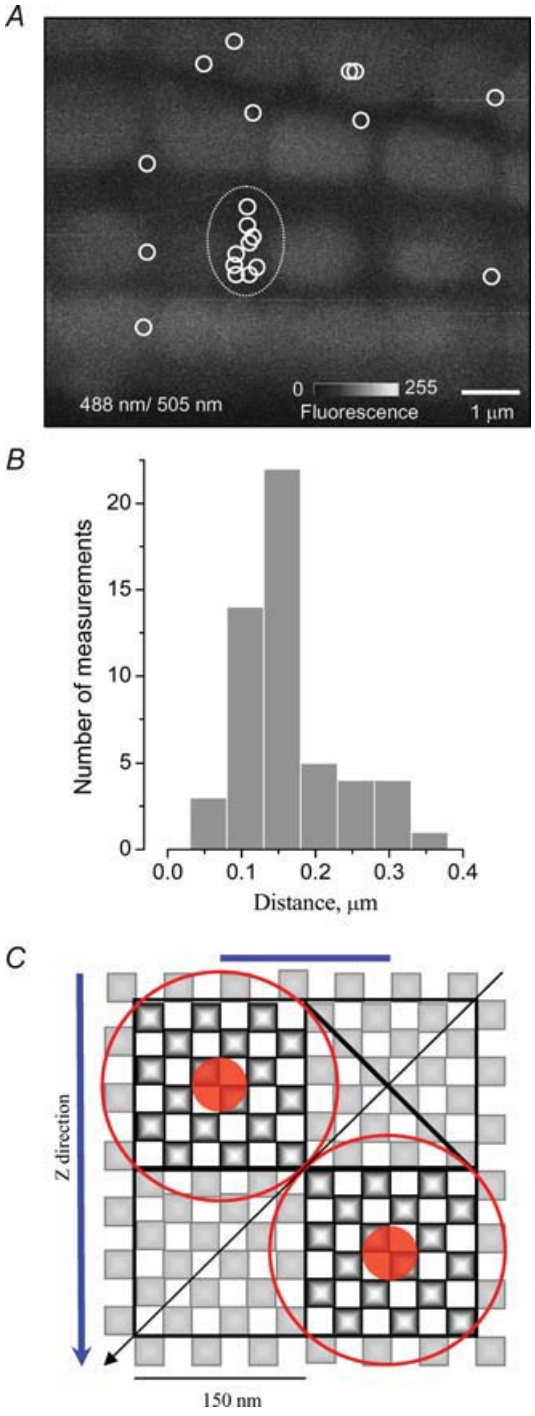

Figure 10. Repetitive sparks in ventricular cells
A, disproportionate activity of RyR2 clusters in ventricular cells. Centers of recorded sparks are marked with circles. Ca^{2+} sparks were recorded after pretreatment of permeabilized ventricular cells with 0.1 μM Bodipy-TR-X ryanodine and 25 μM fluo-3 (pentapotassium salt). Excitation/emission, 488/505 nm. Optical slice < 1 μm. *B*, distribution of shortest distances between repetitive sparks ($n = 53$). *C*, the diagram shows distribution of putative functional groups of RyR2s within a RyR2 cluster depending on their shape, square (set of black boxes) or round (red ring). Centres of spark mass are shown with red circles. Blue and black arrows show two points of view in Z direction depending on orientation of the cluster. Blue and black lines show corresponding distances between centres of mass.

root from $2x^2$) and the group will include ~25 RyR2s. Thus, we suggest that the functional group of RyR2s might include 18–25 RyR2s.

Discussion

We investigated the distribution of RyR2s in rat ventricular myocytes using electron microscopy and different immunofluorescence methods. RyR2s are found abundantly at the Z-line as reported widely by others. It is important, however, that RyR2s were also found in the A-band and in the perinuclear region. Furthermore, Ca^{2+} sparks were found at these regions as well, suggesting that functional groups of RyR2s occur in the depth of the ventricular myocyte at non-traditional locations. It is plausible that Z-line Ca^{2+} sparks arise from RyR2 clusters in the jSR whereas the perinuclear Ca^{2+} sparks or sparks in the middle of sarcomere arise from groups of RyR2s in these regions of the SR. Local Ca^{2+} signalling due to these RyR2 clusters is likely to influence mitochondrial and nuclear function in addition to the influence exerted by both normal and pathological global Ca^{2+} signals. Some of the issues and controversies related to our findings are discussed below.

Electron microscopy

Shacklock *et al.* (1995) showed that only 85% of the Ca^{2+} sparks evoked by electrical stimulation occurred within 0.5 μm of a T-tubule in rat ventricular cells. This is similar to the 78% for the same region shown in our experiments for spontaneous Ca^{2+} sparks (Fig. 8*C*). Although, these authors mentioned the possibility of input from the cSR in their experiments (i.e. from voltage-independent sparks), the existence of 15% of sparks between Z-lines could also mean that groups of RyR2s, such as those producing sparks in the jSR, also exist along axial tubules of TATS. To find out whether A-band RyR2s are associated with the jSR along these TATS tubules, we studied TATS contacts on images after conventional fixation followed by Epon embedding. If longitudinal tubules of the TATS have junctions with SR similar to jSR, this should be seen in the middle of the sarcomere as well as jSR around T-tubules. Nevertheless, we found only two structures slightly similar to the jSR.

Although Epon embedding allowed excellent visualization of the most delicate intracellular membrane structures in the PNM zone including the Golgi complex (data not shown), it did not reveal structures similar to RyR2 clusters within the zone of PNM and the A-band zone. However, the feet (i.e. RyR2s; Franzini-Armstrong, 1973) could be seen much better in the junctional cleft due to the very specific organization of RyR2s near the T-tubule membrane and from the penetration of the dye into the body of the section. Clusters of jSR RyR2s organized along the membrane would be easily

recognized without immunostaining because of the specific pattern. However, the clarity of their visualization definitely depends on the angle of the cut. Figure 2*B* shows a slightly oblique section through a T-tubule fully wrapped by the jSR. Note that only five to six out of the possible 17–18 RyR2s are seen around the T-tubule. Oblique sectioning definitely reduces the visualization of other RyR2s. This could result from mechanisms of stain penetration into the body of ultrathin sections. A stain penetrates into the sections primarily through sites where the structure intersects the surface (Shalla *et al.* 1964). Although Epoxy resins bind more strongly to proteins, it is possible that a network of dye channels could appear (as cracks) on the border between the resin and protein during polymeralization (Shalla *et al.* 1964; Peters *et al.* 1971). In other words, due to structural coupling (Marx *et al.* 2001) every RyR2 could be marked with the stain in the body of the section. In this case, the size of the ultrathin section will allow visualization of three layers of RyR2s. However, because of the checkered order and the shadowgram nature of electron microscopy, they will be seen as a chain of darker and lighter bodies, where the former results from sum of two RyR2 homotetramers, and the latter from a *single* RyR2 homotetramer. If this is true, the single RyR2 homotetramer has to be relatively invisible on micrographs and this explains the small number of structures similar to the feet found in the middle of the sarcomere. Note that this number is not proportional to ∼20% of Ca^{2+} sparks we found in this zone.

Sparks are produced by groups of at least 10 RyR2s (Lukyanenko *et al.* 2000). Therefore, it is very important that our electron microscopy approach allowed us to reveal nSR platforms in the middle of the sarcomere, where groups of up to 20 RyR2s could be located (Fig. 1*C*). It is interesting that the middle of the sarcomere is a place where the nSR can be relatively stable in a contracting ventricular cell. Figure 1*D* shows that some mitochondria have an invagination filled with nSR in the middle of the sarcomere. Independent of the nature of the invagination (this could be an artifact of the preparation for electron microscopy), this demonstrates that M-rete has intimate contact with mitochondria.

Localization of RyR2s with immunofluorescence

We used ventricular cells permeabilized with saponin before or after fixation. The labels were located not only along Z-lines, but also along the myofibrils and within the A-band (i.e. in the nSR; Fig. 4*A*). Longitudinal bands between Z-lines may not represent portions of the axial T-tubules filled with secondary antibodies because control experiments did not show any clear fluorescence from this region (Fig. 4*B*). Recently Chen-Izu *et al.* (2006) also showed the existence of RyR2s in the middle of the ventricular sarcomere but only in regions close to the outer membrane. After fixation and long-term delivery of antibodies we found a similar distribution of RyR2s in the whole cell (Fig. 4*C* and *D*). Deconvolved images from cells after fixation in paraformaldehyde (Fig. 4*C* and *D*) showed clear fluorescence from the A-band and the PNM zone.

Earlier a similar longitudinal distribution of fluorescent labelling was shown only for SERCA (Jorgensen *et al.* 1982) and phospholamban (Jorgensen & Jones, 1987). Thus, to have additional evidence for RyR2 location between the Z-lines, we performed immunostaining for calsequestrin. Calsequestrin was shown to be associated structurally and functionally linked to RyR2s (Jones *et al.* 1995; Sitsapesan & Williams, 1997; Györke *et al.* 2004). The distribution of calsequestrin appears similar to the distribution of RyR2s in our experiments. Double labelling for RyR2s and calsequestrin (two experiments; data not shown) also confirmed their colocalization.

Unfortunately, we cannot conclude anything about the proportion of Z-lines and A-band RyR2s because of significant restrictions in the diffusion of antibodies to the junctional cleft and to the middle of the sarcomere (Parfenov *et al.* 2006). In addition, weak longitudinal and strong transverse labelling of RyR2s could result from differences in longitudinal and transverse diffusion of IgGs. A similar distribution was shown earlier for particles $\geq$ 6 nm within 10 min after entering a permeabilized ventricular cell (Parfenov *et al.* 2006), for glycogen granules in intact ventricular cells (Fawcett & McNutt, 1969), and for enhanced green fluorescent protein expressed in isolated ventricular cells (Salnikov *et al.* 2007). However, our control experiments showed no signs of such grid labelling when only the secondary antibody was used (Figs 4*B* and 5*B*) or revealed a totally different pattern of labelling when we performed immunolabelling for the cytoskeletal protein α-tubulin (Fig. 5*C*).

Thus, we conclude that our immunofluorescent data showed that RyR2s are localized not only in the junctional cleft, but also in the nSR around IMFMs and around the PNMs.

Comparison of spontaneous Ca^{2+} sparks produced in different cellular subdomains

We imaged Ca^{2+} sparks to find out whether functional groups of RyR2s existed in the middle of the A-band and in the perinuclear region. Such sparks, if found, could have similar or different properties from jSR Ca^{2+} sparks. Without defining function, there is no reason to assume orthodox Ca^{2+} spark behaviour. There were, however, published results on prolonged perinuclear Ca^{2+} signals originating from the Golgi apparatus (Yang & Steele, 2005, 2007) that suggested we would observe non-standard Ca^{2+} sparks.

Ca^{2+} sparks were observed in the A-band region and in the perinuclear region. The sparks from these zones of the cell had a different frequency but generally similar characteristics (Fig. 9*D*) to normal Ca^{2+} sparks. The frequency of PNM sparks was ∼2 times lower than the frequency of sparks in the middle of the sarcomere, and 10 times lower than the frequency of sparks in the Z-line zone. However, the difference in spark frequency cannot be discussed without knowing the proportion of RyR2s in these zones, which unfortunately remains unknown. The much smaller number of RyR2s found within the zones in our immunofluorescence experiments could explain the differences.

Similarity between spatio-temporal characteristics of spontaneous Ca^{2+} sparks from jSR and non-junctional regions were recently shown for atrial cells (Sheehan *et al.* 2006), where input from out-of-focus sparks should be the same for cell centre and periphery. Sparks from the PNM zone had a slightly longer duration in comparison to sparks from Z-line and A-band zones. The ∼25% longer duration of PNM sparks could be explained by (1) input from out-of-focus sparks, (2) by lower Ca^{2+} buffering as a result of the lack of troponin C in the PNM zone, (3) by the activation of additional Ca^{2+} release from mitochondria (Maack *et al.* 2006), and/or (4) by the RyR2s of the Golgi apparatus (Yang & Steele, 2005, 2007). Under our recording conditions, we did not see Ca^{2+} release events with the spatio-temporal characteristics described by Yang & Steele (2005, 2007) (width, ∼5 μm; duration, ∼1.8 s). This inconsistency in results could be ascribed to the significant difference in our experimental solutions.

That we observed normal appearing Ca^{2+} sparks in non-standard locations suggests that a jSR-like organization might be found at the spark site. However, Jorgensen and co-authors (Jorgensen & McGuffee, 1987; Jorgensen *et al.* 1993) showed the absence of calsequestrin in nSR, and that only cSR and jSR contained both calsequestrin and RyR2s. The functional importance of calsequestrin to Ca^{2+} release function was shown by Györke *et al.* (2004) who found that the calsequestrin complex with triadin1 and junctin appears to play a role in the regulation of Ca^{2+} leak through RyR2s in ventricular cells. Calsequestrin is thought to inhibit RyR2s by decreasing the amplitude and duration of sparks and the combination of the calsequestrin–triadin–junctin complex with RyR2s enables the RyR2 gating to be affected by changes in $[Ca^{2+}]$ in the SR lumen, an important feature of normal Ca^{2+} spark behaviour (Lukyanenko *et al.* 1996, 1998, 2000, 2001). In other words, without RyR2s bound to calsequestrin, Ca^{2+} sparks in the middle of the sarcomere must have higher amplitude and frequency than sparks from the Z-line zone. Our finding of similarity between sarcomeric sparks tends to support the idea that calsequestrin and RyR2s are colocalized also in the middle of sarcomere.

The question remains what physical and functional structures can account for our observations. Could nSR platforms in the middle of sarcomere be responsible for the non-standard Ca^{2+} sparks? While the cSR may not be in the middle of the A-band, a recent report suggests that the location of cSR is broader than previously thought (Franzini-Armstrong *et al.* 2005).

As discussed above, the nSR platforms could provide space for a group of about 20 RyR2s. Our analysis showed that a functional group of RyR2s producing a spark could be approximately 18–25 RyR2s. Originally Cheng *et al.* (1993) estimated that Ca^{2+} flow associated with spark is ∼40 fC and proposed that it could be induced by single RyR2 (4 pA during 10 ms). However, later it was shown that under near-physiological ionic conditions the Ca^{2+} current through the single RyR2 is less than 0.4 pA (Mejia-Alvarez *et al.* 1999; Kettlun *et al.* 2003). Reduction of time of underlying Ca^{2+} flow to 4 ms (Bers, 2001) increased number of channels contributing to the single spark to 20 RyR2s. Specific experiments (Lukyanenko *et al.* 2000) and calculations (Soeller & Cannell, 2002) performed to find the number of RyR2s underlying Ca^{2+} sparks resulted in suggestions of 10–13 RyR2s. Thus, our numbers are in good agreement with previous results and support the existence of ultrastructural RyR2 unit producing elementary Ca^{2+} release. The difference between the minimum number of RyR2s and our 18–25 RyR2s suggests the possible existence of non-functional RyR2s. They could be located on the border of the group. Such RyR2s could be permanently in a blocked conformational state. In this case coupling between RyR2s could exist only within the borders of the non-functional RyR2s. This could partially explain the functional integrity of the group.

Possible role for non-junctional clusters of RyR2s located around PNMs and IMFMs

Because of their Ca^{2+} sensitivity, non-junctional RyR2s should be involved in excitation–contraction coupling through Ca^{2+}-induced Ca^{2+} release under some conditions. They of course would not be triggered by L-type Ca^{2+} channels (DHPRs) unless one (or more) is close enough. It should be remembered, however, that DHPRs could still be present in the axial tubules even if we have not yet visualized them. If present and apposed to the RyR2 clusters, DHPRs could trigger A-band Ca^{2+} sparks. We have found no evidence for or against this possibility. As for all Ca^{2+} spark sites, if the SR becomes overloaded with Ca^{2+}, RyR2 instability could develop (Lukyanenko *et al.* 2001) and these A-band RyR2 clusters could contribute to propagating CICR.

The data presented here support our mathematical model prediction (Subramanian *et al.* 2001) for the existence of functional Ca^{2+} release sites between Z-lines in rat ventricular myocytes. This model explored the mechanisms of circular Ca^{2+} wave propagation in ventricular cells. When it was based on the classical scheme for the distribution of Ca^{2+} release sites, it failed to reproduce a circular wave. Only incorporation of 20% of the sites in the middle of a sarcomere would allow the Ca^{2+} wave to spread with roughly the same velocity longitudinally and transversely, according to this model. The 'Ca^{2+} release sites' in the model are not single RyR2s, but groups of RyR2s able to produce elementary Ca^{2+} release (i.e. a spark). The model suggests that about 20% of spontaneous sparks should arise from the middle of the sarcomere. In this manner, during Ca^{2+} overload, the Z band Ca^{2+}-release sites would contribute to arrhythmogenic CICR. Under normal conditions, however, these 'non-orthodox' Ca^{2+}-release sites could contribute to excitation–contraction coupling, to mitochondrial and nuclear signalling and to Ca^{2+}-dependent gene regulation.

Trafficking. Trafficking of proteins in the heart is largely unexplored territory. We should consider the possibility that the perinuclear Ca^{2+} sparks and RyR2s found there may reflect trafficking elements that have some function. Certainly the large size and organization of the RyR2 at the jSR suggests that special issues regarding the trafficking of these proteins may exist. The replacement of aged proteins in huge junctional clusters of RyR2s would be clumsy if not impossible. Recently we showed (Parfenov *et al.* 2006) that the junctional cleft in permeabilized ventricular cells is not available even for 3 nm particles. Meanwhile, each RyR2 homotetramer itself has dimensions of about 28 nm × 28 nm × 23 nm (Sharma *et al.* 1998) and some of the regulatory proteins for RyR2s may be as large as 10 nm in diameter (proteins with molecular weights of 62–156 kDa were shown to have a radius of 3.4–7.2 nm; Vandegriff *et al.* 1997). Therefore, it is possible (likely) that the complexes between RyR2s and regulatory proteins are assembled outside of the junctional cleft.

References

Bers DM (2001). *Excitation-Contraction Coupling and Cardiac Contractile Force*. Kluwer Academic Publishers, Dordrecht, The Netherlands.

Bers DM (2004). Macromolecular complexes regulating cardiac ryanodine receptor function. *J Mol Cell Cardiol* **37**, 417–429.

Bhat MB, Hayek SM, Zhao J, Zang W, Takeshima H, Wier WG & Ma J (1999). Expression and functional characterization of the cardiac muscle ryanodine receptor Ca^{2+} release channel in Chinese hamster ovary cells. *Biophys J* **77**, 808–816.

Bilmen JG, Wootton LL & Michelangeli F (2002). The inhibition of the sarcoplasmic/endoplasmic reticulum Ca^{2+}-ATPase by macrocyclic lactones and cyclosporin A. *Biochem J* **366**, 255–263.

Bridge JH, Ershler PR & Cannell MB (1999). Properties of Ca^{2+} sparks evoked by action potentials in mouse ventricular myocytes. *J Physiol* **518**, 469–478.

Brochet DX, Yang D, Di Maio A, Lederer WJ, Franzini-Armstrong C & Cheng H (2005). Ca^{2+} blinks: rapid nanoscopic store calcium signaling. *Proc Natl Acad Sci U S A* **102**, 3099–3104.

Carl SL, Felix K, Caswell AH, Brandt NR, Ball WJ, JrVaghy PL, Meissner G & Ferguson DG (1995). Immunolocalization of sarcolemmal dihydropyridine receptor and sarcoplasmic reticular triadin and ryanodine receptor in rabbit ventricle and atrium. *J Cell Biol* **129**, 672–682.

Cheng H, Lederer W & Cannell M (1993). Calcium sparks: elementary events underlying excitation-contraction coupling in heart muscle. *Science* **262**, 740–744.

Chen-Izu Y, McCulle SL, Ward CW, Soeller C, Allen BM, Rabang C, Cannell MB, Balke CW & Izu LT (2006). Three-dimensional distribution of ryanodine receptor clusters in cardiac myocytes. *Biophys J* **91**, 1–13.

Chinopoulos C, Lederer WJ & Lukyanenko V (2005). Visualization of mitochondrial intermembrane space with fluo-3 (K^+) in isolated rat ventricular cardiomyocytes. *Biophys J* **88**, 87a.

Dolber PC & Sommer JR (1984). Corbular sarcoplasmic reticulum of rabbit cardiac muscle. *J Ultrastruct Res* **87**, 190–196.

DuBell WH, Lederer WJ & Rogers TB (2000). K^+ currents responsible for repolarization in mouse ventricle and their modulation by FK-506 and rapamycin. *Am J Physiol Heart Circ Physiol* **278**, H886–H897.

Fabiato A (1985). Time and calcium dependence of activation and inactivation of calcium-induced release of calcium from the sarcoplasmic reticulum of a skinned canine cardiac Purkinje cell. *J Gen Physiol* **85**, 247–289.

Fawcett DW & McNutt NS (1969). The ultrastructure of the cat myocardium. I. Ventricular papillary muscle. *J Cell Biol* **42**, 1–45.

Frank JS (1990). Ultrastructure of the unfixed myocardial sarcolemma and cell surface. In *Calcium and the Heart*, ed. Langer GA, pp. 1–25. Raven Press, New York.

Franzini-Armstrong C (1973). Studies of the triad. IV. Structure of the junction in frog slow fibers. *J Cell Biol* **56**, 120–128.

Franzini-Armstrong C, Protasi F & Ramesh V (1999). Shape, size, and distribution of Ca^{2+} release units and couplons in skeletal and cardiac muscles. *Biophys J* **77**, 1528–1539.

Franzini-Armstrong C, Protasi F & Tijskens P (2005). The assembly of calcium release units in cardiac muscle. *Ann NY Acad Sci* **1047**, 76–85.

Györke I, Hester N, Jones LR & Györke S (2004). The role of calsequestrin, triadin, and junctin in conferring cardiac ryanodine receptor responsiveness to luminal calcium. *Biophys J* **86**, 2121–2128.

Györke S, Lukyanenko V & Györke I (1997). Dual effects of tetracaine on spontaneous calcium release in rat ventricular myocytes. *J Physiol* **500**, 297–309.

Inui M, Saito A & Fleischer S (1987). Isolation of the ryanodine receptor from cardiac sarcoplasmic reticulum and identity with the feet structures. *J Biol Chem* **262**, 15637–15642.

Jones LR, Zhang L, Sanborn K, Jorgensen AO & Kelley J (1995). Purification, primary structure, and immunological characterization of the 26-kDa calsequestrin binding protein (junctin) from cardiac junctional sarcoplasmic reticulum. *J Biol Chem* **270**, 30787–30796.

Jorgensen AO & Jones LR (1987). Immunoelectron microscopical localization of phospholamban in adult canine ventricular muscle. *J Cell Biol* **104**, 1343–1352.

Jorgensen AO & McGuffee LJ (1987). Immunoelectron microscopic localization of sarcoplasmic reticulum proteins in cryofixed, freeze-dried, and low temperature-embedded tissue. *J Histochem Cytochem* **35**, 723–732.

Jorgensen AO, Shen AC, Arnold W, McPherson PS & Campbell KP (1993). The Ca^{2+}-release channel/ryanodine receptor is localized in junctional and corbular sarcoplasmic reticulum in cardiac muscle. *J Cell Biol* **120**, 969–980.

Jorgensen AO, Shen AC, Daly P & MacLennan DH (1982). Localization of Ca^{2+} + Mg^{2+}-ATPase of the sarcoplasmic reticulum in adult rat papillary muscle. *J Cell Biol* **93**, 883–892.

Kettlun C, Gonzalez A, Rios E & Fill M (2003). Unitary Ca^{2+} current through mammalian cardiac and amphibian skeletal muscle ryanodine receptor channels under near-physiological ionic conditions. *J Gen Physiol* **122**, 407–417.

Lai FA, Anderson K, Rousseau E, Liu QY & Meissner G (1988). Evidence for a Ca^{2+} channel within the ryanodine receptor complex from cardiac sarcoplasmic reticulum. *Biochem Biophys Res Commun* **151**, 441–449.

Lopez-Lopez J, Shacklock P, Balke CW & Wier WG (1995). Local calcium transients triggered by single L-type calcium channel currents in cardiac cells. *Science* **268**, 1042–1045.

Lukyanenko V & Györke S (1999). Ca^{2+} sparks and Ca^{2+} waves in saponin-permeabilized cardiac myocytes. *J Physiol* **521**, 575–585.

Lukyanenko V, Györke I & Györke S (1996). Regulation of calcium release by calcium inside the sarcoplasmic reticulum in ventricular myocytes. *Pflugers Arch* **432**, 1047–1054.

Lukyanenko V, Györke I, Subramanian S, Smirnov A, Wiesner TF & Györke S (2000). Inhibition of Ca^{2+} sparks by ruthenium red in permeabilized rat ventricular myocytes. *Biophys J* **79**, 1273–1284.

Lukyanenko V, Viatchenko-Karpinski S, Smirnov A, Wiesner TF & Györke S (2001). Dynamic regulation of the SR Ca^{2+} content by lumenal Ca^{2+}-sensitive leak through RyR2s in rat ventricular myocytes. *Biophys J* **81**, 785–798.

Lukyanenko V, Wiesner TF & Györke S (1998). Termination of Ca^{2+} release during Ca^{2+} sparks in rat ventricular myocytes. *J Physiol* **507**, 667–677.

Maack C, Cortassa S, Aon MA, Ganesan AN, Liu T & O'Rourke B (2006). Elevated cytosolic Na^{+} decreases mitochondrial Ca^{2+} uptake during excitation-contraction coupling and impairs energetic adaptation in cardiac myocytes. *Circ Res* **99**, 172–182.

Marx SO, Gaburjakova J, Gaburjakova M, Henrikson C, Ondrias K & Marks AR (2001). Coupled gating between cardiac calcium release channels (ryanodine receptors). *Circ Res* **88**, 1151–1158.

Marx SO, Reiken S, Hisamatsu Y, Jayaraman T, Burkhoff D, Rosemblit N & Marks AR (2000). PKA phosphorylation dissociates FKBP12.6 from the calcium release channel (ryanodine receptor): defective regulation in failing hearts. *Cell* **101**, 365–376.

Maunsbach AB & Afzelius BA (1999). *Biomedical Electron Microscopy*. Academic Press, New York.

Mejia-Alvarez R, Kettlun C, Rios E, Stern M & Fill M (1999). Unitary Ca^{2+} current through cardiac ryanodine receptor channels under quasi-physiological ionic conditions. *J Gen Physiol* **113**, 177–186.

Newman GR & Hobot JA (1993). *Resin Microscopy and on-Section Immunocytochemistry*. Springer-Verlag, New York.

Parfenov AS, Salnikov V, Lederer WJ & Lukyanenko V (2006). Aqueous diffusion pathways as a part of the ventricular cell ultrastructure. *Biophys J* **90**, 1107–1119.

Peters A, Hinds PL & Vaughn JE (1971). Extent of stain penetration in sections prepared for electron microscopy. *J Ultrastruct Res* **36**, 37–45.

Pratusevich VR & Balke CW (1996). Factors shaping the confocal image of the calcium spark in cardiac muscle cells. *Biophys J* **71**, 2942–2957.

Salnikov VV, Lukyanenko YO, Frederick CA, Lederer WJ & Lukyanenko VI (2007). Probing the outer mitochondrial membrane in cardiac mitochondria with nanoparticles. *Biophys J* **92**, 1058–1071.

Scriven DR, Klimek A, Asghari P, Bellve K & Moore ED (2005). Caveolin-3 is adjacent to a group of extradyadic ryanodine receptors. *Biophys J* **89**, 1893–1901.

Sedarat F, Lin E, Moore ED & Tibbits GF (2004). Deconvolution of confocal images of dihydropyridine and ryanodine receptors in developing cardiomyocytes. *J Appl Physiol* **97**, 1098–1103.

Shacklock PS, Wier WG & Balke CW (1995). Local Ca^{2+} transients (Ca^{2+} sparks) originate at transverse tubules in rat heart cells. *J Physiol* **487**, 601–608.

Shalla TA, Carroll TW & Dezoeten GA (1964). Penetration of stain in ultrathin sections of tobacco mosaic virus. *Stain Technol* **39**, 257–265.

Sharma MR, Penczek P, Grassucci R, Xin HB, Fleischer S & Wagenknecht T (1998). Cryoelectron microscopy and image analysis of the cardiac ryanodine receptor. *J Biol Chem* **273**, 18429–18434.

Sheehan KA, Zima AV & Blatter LA (2006). Regional differences in spontaneous Ca^{2+} spark activity and regulation in cat atrial myocytes. *J Physiol* **572**, 799–809.

Sitsapesan R & Williams AJ (1997). Regulation of current flow through ryanodine receptors by luminal Ca^{2+}. *J Membr Biol* **159**, 179–185.

Sobie EA, Dilly KW, dos Santos Cruz J, Lederer WJ & Jafri MS (2002). Termination of cardiac Ca^{2+} sparks: an investigative mathematical model of calcium-induced calcium release. *Biophys J* **83**, 59–78.

Soeller C & Cannell MB (1999). Examination of the transverse tubular system in living cardiac rat myocytes by 2-photon microscopy and digital image-processing techniques. *Circ Res* **84**, 266–275.

Soeller C & Cannell MB (2002). Estimation of the sarcoplasmic reticulum Ca^{2+} release flux underlying Ca^{2+} sparks. *Biophys J* **82**, 2396–2414.

Soeller C, Gilbert R, Song X & Cannell MB (2006). An immunocytochemical study of the morphology of RyR2 clusters in rat ventricular myocytes. *Biophys J* **90**, 556a.

Sommer JR & Johnson EA (1968). Cardiac muscle. A comparative study of Purkinje fibers and ventricular fibers. *J Cell Biol* **36**, 497–526.

Subramanian S, Viatchenko-Karpinski S, Lukyanenko V, Györke S & Wiesner TF (2001). The underlying mechanisms of symmetric calcium wave propagation in rat ventricular myocytes. *Biophys J* **80**, 1–11.

Vandegriff KD, McCarthy M, Rohlfs RJ & Winslow RM (1997). Colloid osmotic properties of modified hemoglobins: chemically cross-linked versus polyethylene glycol surface-conjugated. *Biophys Chem* **69**, 23–30.

Viatchenko-Karpinski S, Terentyev D, Györke I, Terentyeva R, Volpe P, Priori SG, Napolitano C, Nori A, Williams SC, Györke S (2004). Abnormal calcium signaling and sudden cardiac death associated with mutation of calsequestrin. *Circ Res* **94**, 471–477.

Wehrens XH, Lehnart SE & Marks AR (2005). Intracellular calcium release and cardiac disease. *Annu Rev Physiol* **67**, 69–98.

Xiao RP, Valdivia HH, Bogdanov K, Valdivia C, Lakatta EG & Cheng H (1997). The immunophilin FK506-binding protein modulates Ca^{2+} release channel closure in rat heart. *J Physiol* **500**, 343–354.

Yang Z & Steele DS (2005). Characteristics of prolonged Ca^{2+} release events associated with the nuclei in adult cardiac myocytes. *Circ Res* **96**, 82–90.

Yang Z & Steele DS (2007). Evidence that prolonged nuclear Ca^{2+} release events originate from the Golgi apparatus in rat ventricular myocytes. *Biophys J* **92**, 257a.

Yin CC, Blayney LM & Lai FA (2005). Physical coupling between ryanodine receptor-calcium release channels. *J Mol Biol* **349**, 538–546.

Acknowledgements

This work was supported by grants from American Heart Association (AHA 0060088Y to V.L.) and the National Institutes of Health (HL36974, HL70709, HL67849 and HL25675 to W.J.L.).

Author's permanent address

V. Salnikov: Kazan Institute of Biochemistry and Biophysics, Kazan Science Center, Russian Academy of Sciences, 2/31 Lobachevskii St., Kazan, Russia 420111.